ARMY RESEARCH LABORATORY

An Assessment of the Performance of the History Variable Reactive Burn Explosive Initiation Model in the CTH Code

by John Starkenberg
and Toni M. Dorsey

ARL-TR-1667 May 1998

The findings in this report are not to be construed as an official Department of the Army position unless so designated by other authorized documents.

Citation of manufacturer's or trade names does not constitute an official endorsement or approval of the use thereof.

Destroy this report when it is no longer needed. Do not return it to the originator.

Army Research Laboratory
Aberdeen Proving Ground, MD 21005-5066

ARL-TR-1667 **May 1998**

An Assessment of the Performance of the History Variable Reactive Burn Explosive Initiation Model in the CTH Code

John Starkenberg, Toni M. Dorsey
Weapons and Materials Research Directorate, ARL

Abstract

We exercised the History Variable Reactive Burn (HVRB) model in the CTH code, simulating a number of common explosive sensitivity experiments, including sustained- and pulsed-shock initiation, projectile-impact initiation, and detonation failure. Predictions of sustained-shock initiation are accurate in accordance with the calibration of the model. Predictions of pulsed-shock initiation are only somewhat more accurate than those achieved previously using Forest Fire. Predictions of projectile-impact initiation are much better. The results for bare explosive show excellent agreement with experiment for both flat- and round-tipped projectiles. With a 2-mm tantalum cover, the agreement is nearly as good. With a 6-mm tantalum cover, the agreement deteriorates for flat-tipped projectiles, while remaining adequate in the case of round-tipped projectiles. The failure radius and thickness predicted with CTH exhibit minimam (near which the solutions are most stable) as functions of zone dimension, but do not appear to converge. These minimum values agree well with experiment. Although no converged solutions were obtained, the most stable failure thickness is approximately equal to the most stable failure radius.

Table of Contents

INTENTIONALLY LEFT BLANK.

List of Figures

INTENTIONALLY LEFT BLANK.

List of Tables

INTENTIONALLY LEFT BLANK.

1. Background

A number of different explosive initiation models implemented in continuum mechanics computer programs (commonly called hydrocodes) have been offered over the years. We have used the Forest Fire model (Mader 1970, 1979; Mader and Forest 1976; Lundstrom 1988) in the 2DE code (Kershner and Mader 1972) on many occasions and developed a model of our own that we implemented in a one-dimensional code called ODES (Starkenberg 1989). Because 2DE is a relatively old program, lacking many modern amenities, including modern material modeling capabilities, we were seeking alternatives for reactive modeling applications.

Several choices for the explosive-initiation modeler now exist. For example, another early model called Ignition and Growth (Lee and Tarver 1980) has been incorporated into DYNA. A modified version of Forest Fire is available in SMERF (Lundstrom 1988). More recently, both Forest Fire and JTF (a more sophisticated model named for its creators [Johnson, Tang, and Forest 1985]) have been implemented in the three-dimensional version of the MESA/PAGOSA code. In addition to Forest Fire and Ignition and Growth, the CTH code (Hertel et al. 1993) offers the rather redundantly named History Variable Reactive Burn (HVRB) model (Kerley 1992). These models are all limited in the type of explosive initiation they apply to. They are useful for treating problems of shock-to-detonation transition (SDT), often called shock initiation. Models for more complex scenarios involving deflagration-to-detonation transition (DDT) have been attempted. Most of these are limited to specific experimental arrangements. One model attempting to treat general geometries was developed by Baer and Nunziato (1989), but it exhibits some difficulties (Menikoff 1996).

The most up-to-date of these codes are MESA and CTH. Because reactive modeling was only available in the three-dimensional version of MESA and there appears to be a general preference for use of CTH at the U.S. Army Research Laboratory (ARL), we focused on the latter. Using CTH, we performed computations simulating a variety of shock-initiation experiments and compared the computed results with those of the experiments, as well as those obtained from computations with

other codes. The experiments simulated include sustained- and pulsed-shock initiation, projectile-impact initiation, and detonation failure.

2. Discussion of CTH and the HVRB Model

CTH is an ongoing project of Sandia National Laboratories (SNL). It is intended to provide capabilities for modeling dynamics of multidimensional systems with multiple materials, large deformations, and strong shock waves. Finite-difference analogs of the Lagrangian equations of momentum and energy conservation are employed with continuous rezoning to construct Eulerian differencing. Shock and detonation waves are treated using the method of artificial viscosity. CTH makes use of analytic (Mie-Grüneisen, JWL, etc.) and tabular (Sesame) equations of state, as well as modern constitutive models (Johnson-Cook, Zerilli-Armstrong) including fracture (void insertion). In addition, three reaction and two porosity models are included. These options provide an opportunity to treat complex material behavior, including melting, vaporization, solid-phase transitions, chemical reaction, and electronic excitation and ionization.

The reaction models are the Programmed Burn and CJ Volume Burn models for detonation propagation, and the HVRB model for shock initiation. The Programmed Burn model forces detonation at the characteristic propagation velocity through a specified portion of the computational mesh, while the CJ Volume Burn model permits representation of self-propagating detonation. The HVRB model (Kerley 1992) is designed to treat the process of initiation of detonation in shock-loaded high explosives.

In CTH, chemical reaction is described by a single-reaction progress variable, λ, which is assumed to be a function of a history variable, ϕ.

$$\lambda = \lambda(\phi),$$

where

$$\phi = \int_0^t \Phi(\rho, e, p, T, \ldots) d\tau,$$

and CTH integrates $\Phi(t)$ rather than $\lambda(t)$. Specific forms for Φ and λ are suggested by the fact that the sensitivity of many explosives to initiation by pulsed shock waves exhibits a dependence on the square of the shock pressure multiplied by the pulse duration. Thus,

$$\Phi = \frac{1}{\tau_o} \left(\frac{p - p_I}{p_R} \right)^Z,$$

and

$$\lambda = \phi^M.$$

Here, τ_o, which is used to make ϕ nondimensional, is taken to be equal to 1 μs, and M, p_I (the threshold pressure for reaction), p_R, and Z are constants that may be calibrated to duplicate the shock-initiation behavior of each specific high explosive. Calibration is accomplished with reference to simple sensitivity data characterizing an explosive collected in the wedge test. Data from such tests are generally presented in the form of plots of distance of run and time to detonation as a function of the initial pressure of the shock wave. The former of these is known as the Pop plot (Ramsay and Popolato 1965). Calibrations for several high explosives have been obtained and are distributed with CTH. In applying HVRB, it is important to remember that real explosives exhibit modes of initiation in addition to shock initiation as described by the model.

As has become common practice, CTH treats the reacting explosive as a two-phase mixture of reactants and products. When this is done, available equations of state for the phases may be used. However, since the independent state variables are known only for the mixture, additional equilibrium conditions are required to provide a closed system of equations that can be solved for the dependent state variables. In some codes, the phases are assumed to be in mechanical and thermal equilibrium (Mader 1979). That is, they are assumed to have equal pressures and temperatures. Generally, the times required to achieve thermal equilibrium (via conduction) are

significantly longer than those required to achieve mechanical equilibrium (via wave propagation). Therefore, the condition of mechanical equilibrium can be satisfied more often than the condition of thermal equilibrium. Because of this, the condition of adiabatic reaction has sometimes been used to supplant thermal equilibrium (Johnson, Tang, and Forest 1985; Starkenberg 1989). A significant disadvantage of any such procedure is the requirement for time-consuming iterative computations in order to satisfy the closure conditions. CTH, however, takes neither of these approaches. Rather, the pressure, p, and specific internal energy, e, of the mixture are assumed, without physical justification, to be related to the phase pressures and specific internal energies by the CTH Two-State model:

$$p(\rho, T, \lambda) = (1 - \lambda)\, p_r(\rho, T) + \lambda\, p_p(\rho, T),$$

and

$$e(\rho, T, \lambda) = (1 - \lambda)\, e_r(\rho, T) + \lambda e_p(\rho, T),$$

where the subscripts r and p refer to reactants and products, respectively. Thus, each phase is assumed to have the density and temperature of the mixture. While the latter assumption represents thermal equilibrium, no iterations are required since temperature is an independent variable in the CTH scheme. The mixture pressure and the reaction variable, λ, have no physical definition. The latter "is a generalized variable that combines *both* EOS [equation of state] and reaction rate phenomena" (Kerley 1992). Presumably, such lack of physical fidelity may be compensated for in the calibration process.

During the course of this study, a new version of CTH (June 1996) was released. This version includes several new features including the Forest Fire and Ignition and Growth initiation models. Most importantly, we noticed that somewhat different results were obtained using HVRB in the new version. While these differences were not large, they were significant enough to cause us to rerun all the computations originally made with the earlier version. The results given in this report were obtained using the June 1996 release.

3. General Features of the Simulations

Except in the case of the failure-thickness computations, the simulations reported herein are two-dimensional axisymmetric. Insofar as possible, computational zone dimensions are kept uniform and equal in each coordinate direction in order to maintain square zones. In all cases, exterior boundary conditions are of the "absorbing" type. These boundary conditions permit mass flow into and out of the mesh and produce only weak reflections of incident waves.

4. Sustained-Shock Response of PBX-9404

The initiation response of PBX-9404 has been studied in a wide variety of experiments. Its response to sustained-shock waves, determined in wedge tests (Ramsay and Popolato 1965), forms the basis of the Forest Fire and HVRB calibrations, and these models generally predict sustained-shock response accurately. We reconfirmed the accuracy of the HVRB calibration using two-dimensional axisymmetric simulations and representing sustained-shock initiation by the impact of thick copper flyer plates against the explosive. Impact velocities of 0.55 and 2.00 mm/μs (giving pressures near the upper and lower extremes of the Pop plot) were used.

The thicknesses of the target explosive was chosen to be somewhat greater than the expected distance of run to detonation. The thickness of the flyer was chosen to be half the target thickness, which is sufficient to prevent encroachment of rarefactions from the back of the flyer into the reaction zone. The radii of the target and flyer were chosen equal to the target thickness in order to prevent encroachment of any reflected waves near the axis of symmetry prior to initiation. Two sets of computational zone dimensions were used. One was chosen to give approximately 50 zones over the expected distance of run to detonation, and the other to give about 100 zones. Thus, 0.2- and 0.1-mm square zones were used for the longer run distance, and 0.02- and 0.01-mm square zones were used for the shorter. The results obtained were essentially independent of the zone dimension and provided guidance for the selection of zoning throughout this study.

A sequence of contour plots for the 0.55-mm/μs impact is shown in Figure 1. These give pressure contours to the right of the axis and reaction variable contours to the left with the copper flyer at the bottom. They indicate that reaction begins some distance behind the impact shock and overtakes it to produce transition to detonation. The curvature of the leading wave is associated with reflections from the "absorbing" boundary. Plots of pressure versus distance along the axis of symmetry at various times, shown in Figure 2, indicate that this delayed reaction produces a strong compression or shock wave that overtakes the initial shock (still propagating near its original strength). This behavior is different from that observed using Forest Fire, in which reaction begins immediately behind the initial shock wave and causes it to grow as a square wave during most of the transition process (Starkenberg 1993). The behavior predicted using HVRB is more consistent with experimental observations (Wackerle et al. 1978; Nutt and Erickson 1984). However, experiments do not generally indicate such a strong overtaking compression. Distances of run and times to detonation were determined from plots of pressure versus axial distance at various times. Because of the interval between plots, these are accurate to within about 5%. They are plotted (with error bars) as a function of the initial shock pressure in Figures 3 and 4. While the agreement with the experimental results of Ramsay and Popolato (1965) is, of course, very good, the run and time to detonation at the lower pressure are a little long.

5. Pulsed-Shock Response of PBX-9404

In addition to wedge tests, characterizing the response of PBX-9404 to sustained shock waves, its response to pulsed shock waves has also been determined in experiments using thin Mylar flyer plates (Weingart et al. 1980). The critical impact velocity for initiation was determined as a function of flyer thickness for PBX-9404 charges measuring 25.4 mm in diameter and 19.1 mm in length, laterally enclosed in Plexiglas. Forest Fire has proven inaccurate in predicting these results (Starkenberg 1989).

We used CTH to simulate these experiments in axisymmetric computations with 0.127- and 1.27-mm-thick flyers. In order to accommodate both flyer thicknesses, we used a computational

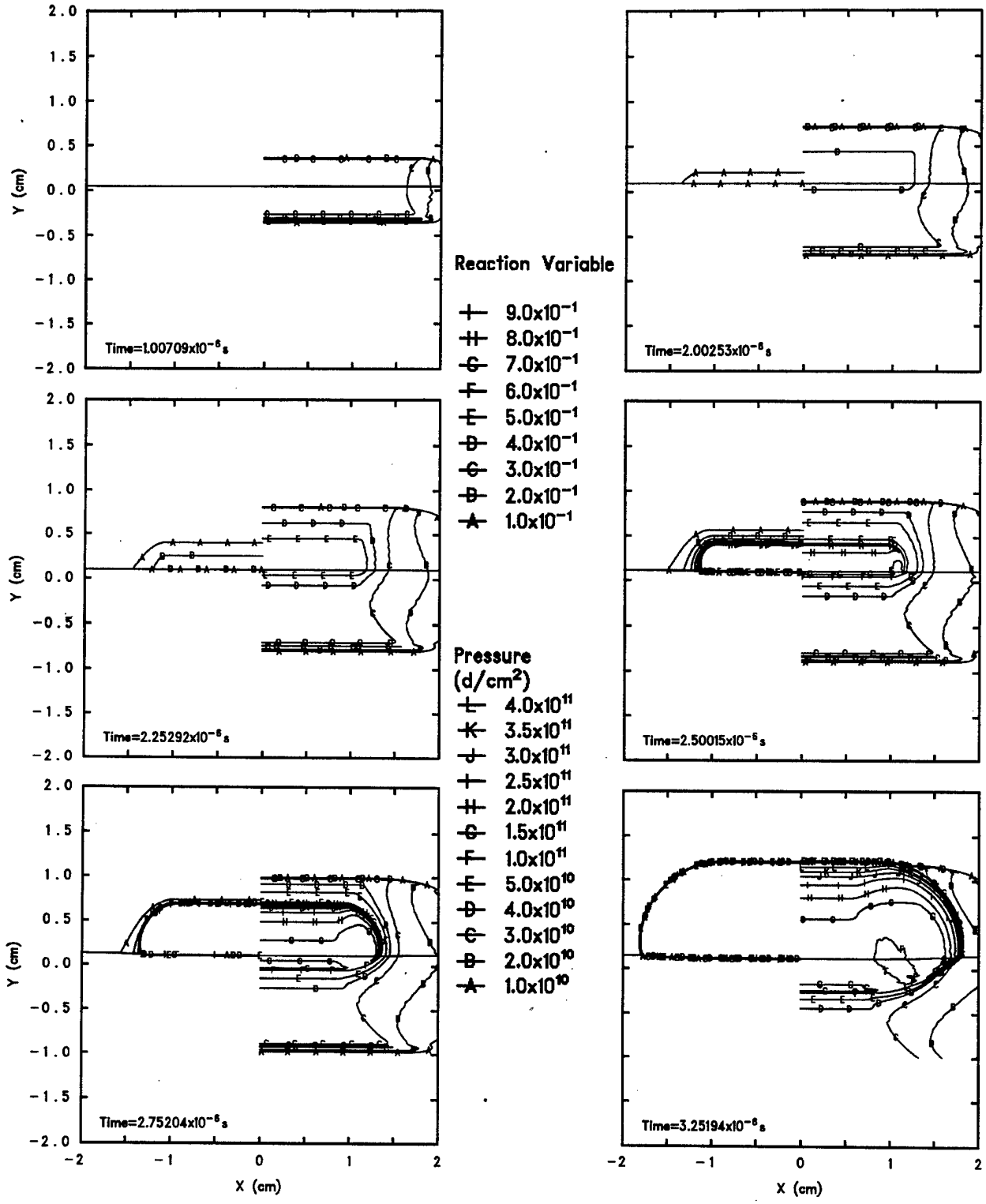

Figure 1. Sequence of Pressure and Reaction Variable Contour Plots for the 0.55-mm/μs Impact of a Thick Copper Flyer Against a Bare PBX-9404 Charge.

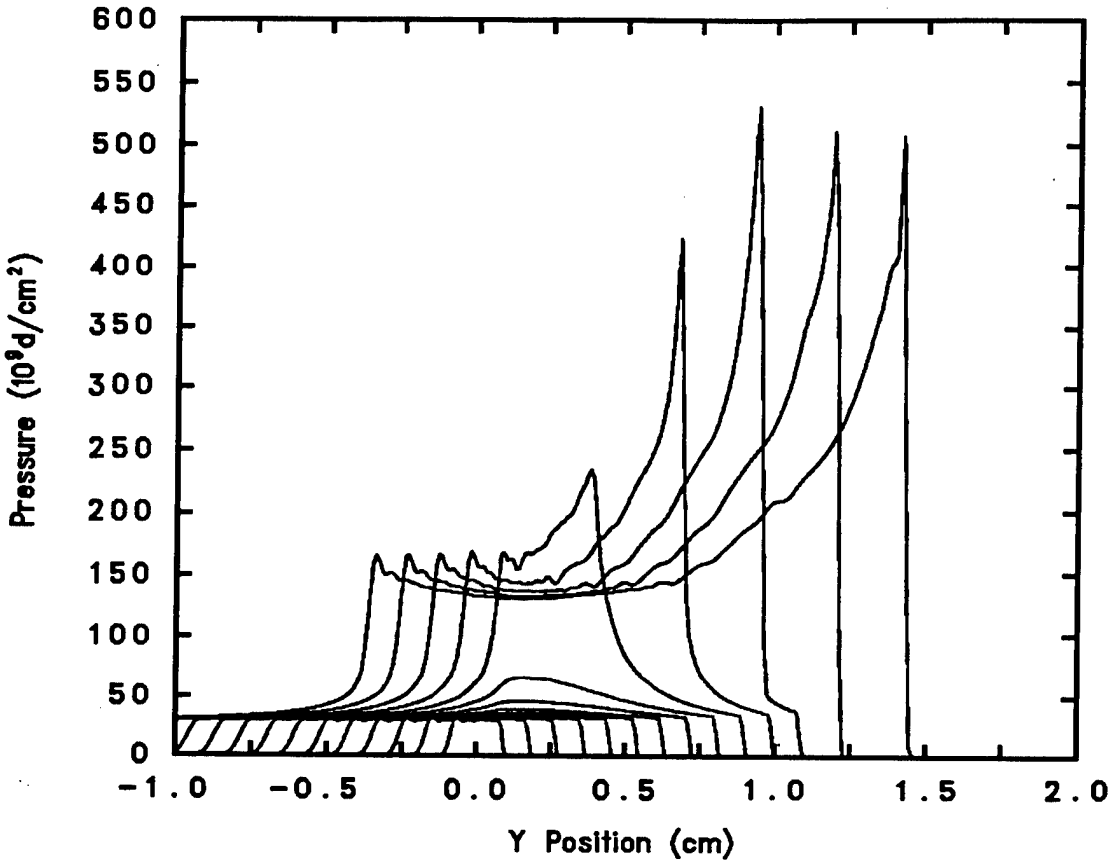

Figure 2. Pressure as a Function of Axial Distance at Several Times Within a PBX-9404 Charge Impacted by a 0.55-mm/μs Copper Flyer.

mesh that is uniform in the radial direction and variable in the axial direction. The radial zone dimension is 0.04 mm and the axial zone dimensions vary between 0.02 mm and 0.08 mm, with the finer zones concentrated near the impact surface. This gives approximately six zones across the thinner flyer. The thicker flyer was also simulated with 0.04-mm square zones without altering the results.

A typical sequence of contour plots leading to initiation is shown in Figure 5. The 1.27-mm-thick Mylar flyer appears at the bottom of the charge. The pressure contours extend into the Plexiglas enclosure. Reaction begins when the wave has traveled about halfway through the charge, and the transition to detonation is rapid. A similar sequence of contour plots at a slightly slower impact velocity is shown in Figure 6. In this case, although some reaction occurs, initiation does not

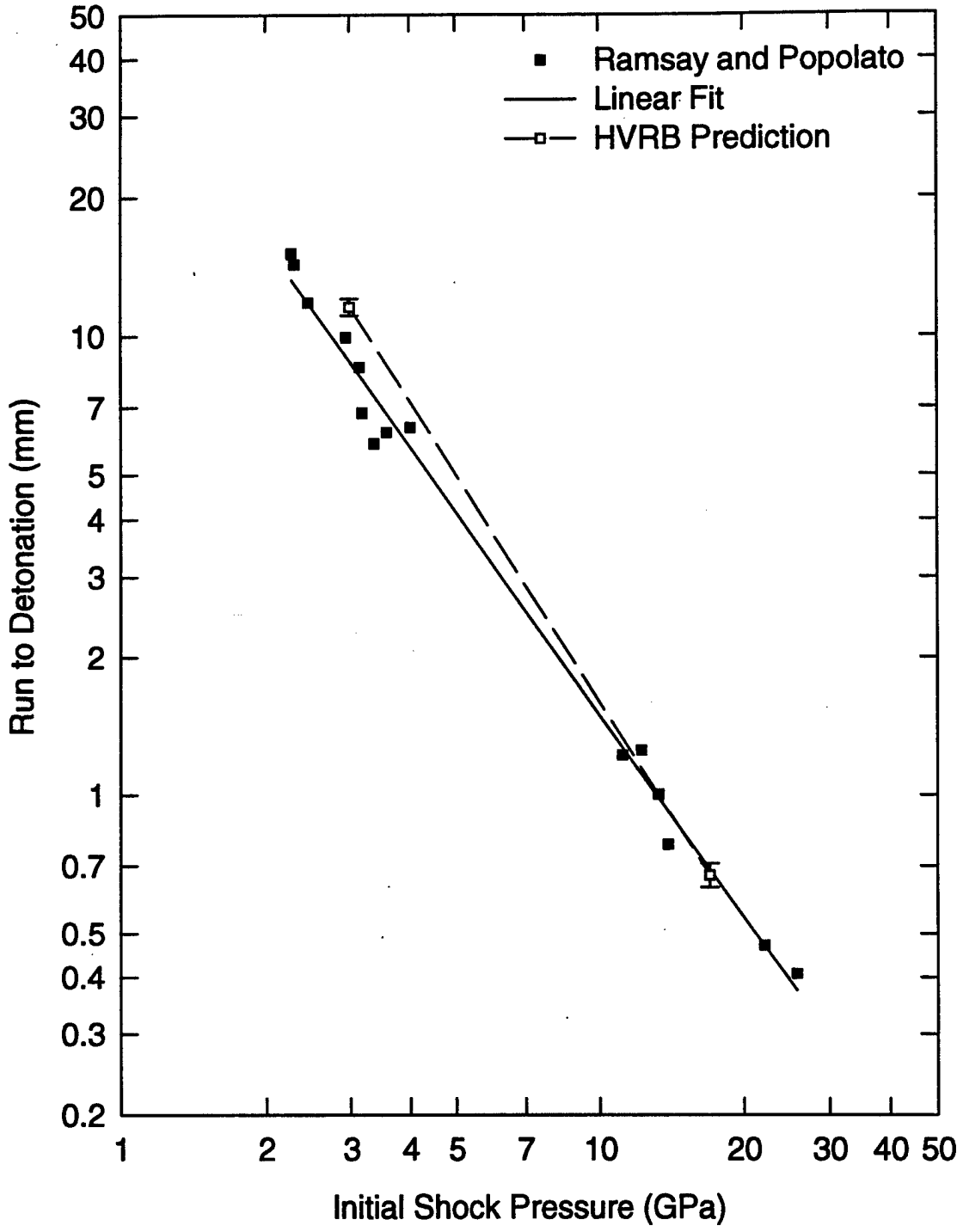

Figure 3. Comparison of HVRB Predictions With Experimental Data for the Distance of Run to Detonation as a Function of the Initial Shock Pressure (Pop Plot).

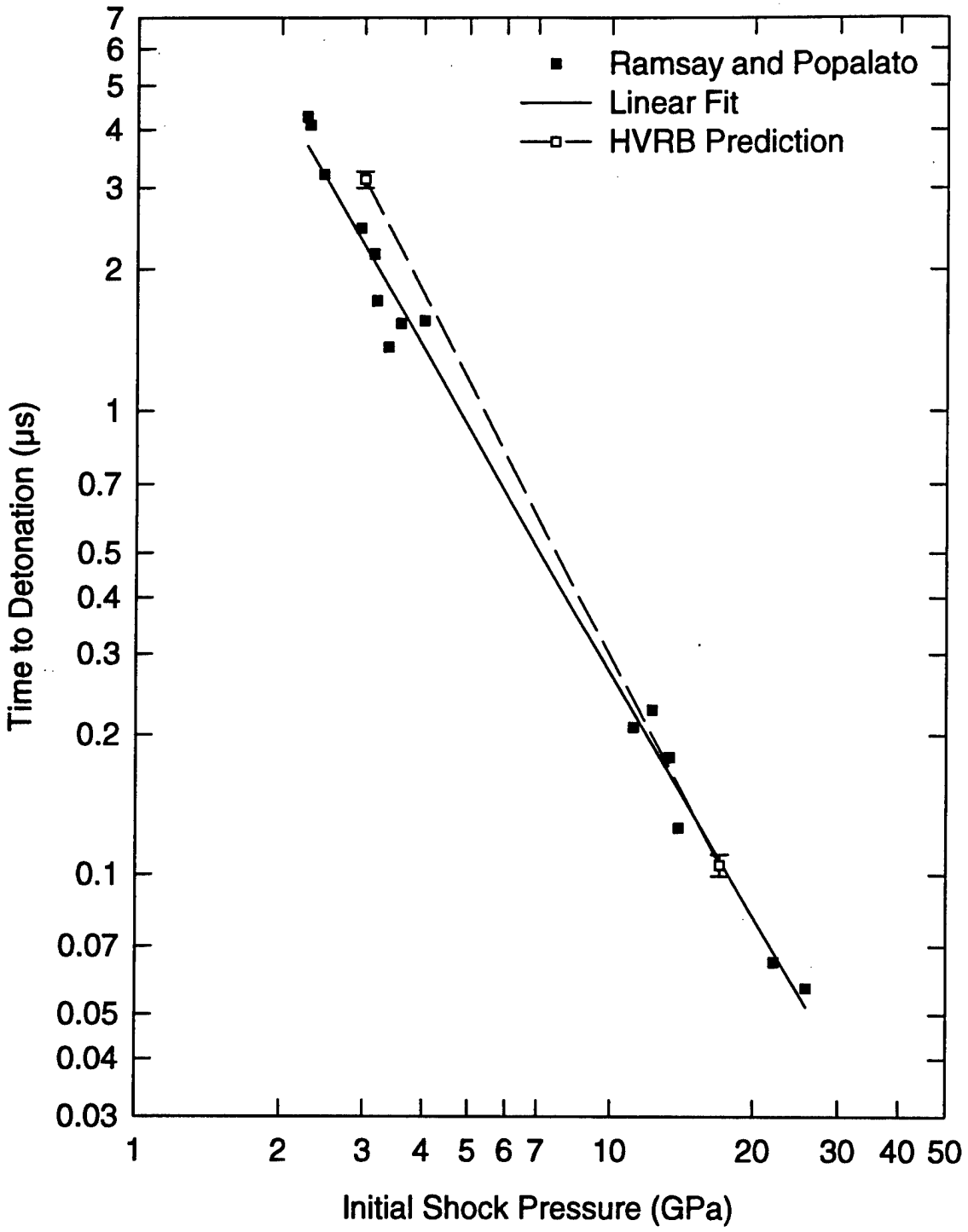

Figure 4. Comparison of HVRB Predictions With Experimental Data for the Time to Detonation as a Function of the Initial Shock Pressure.

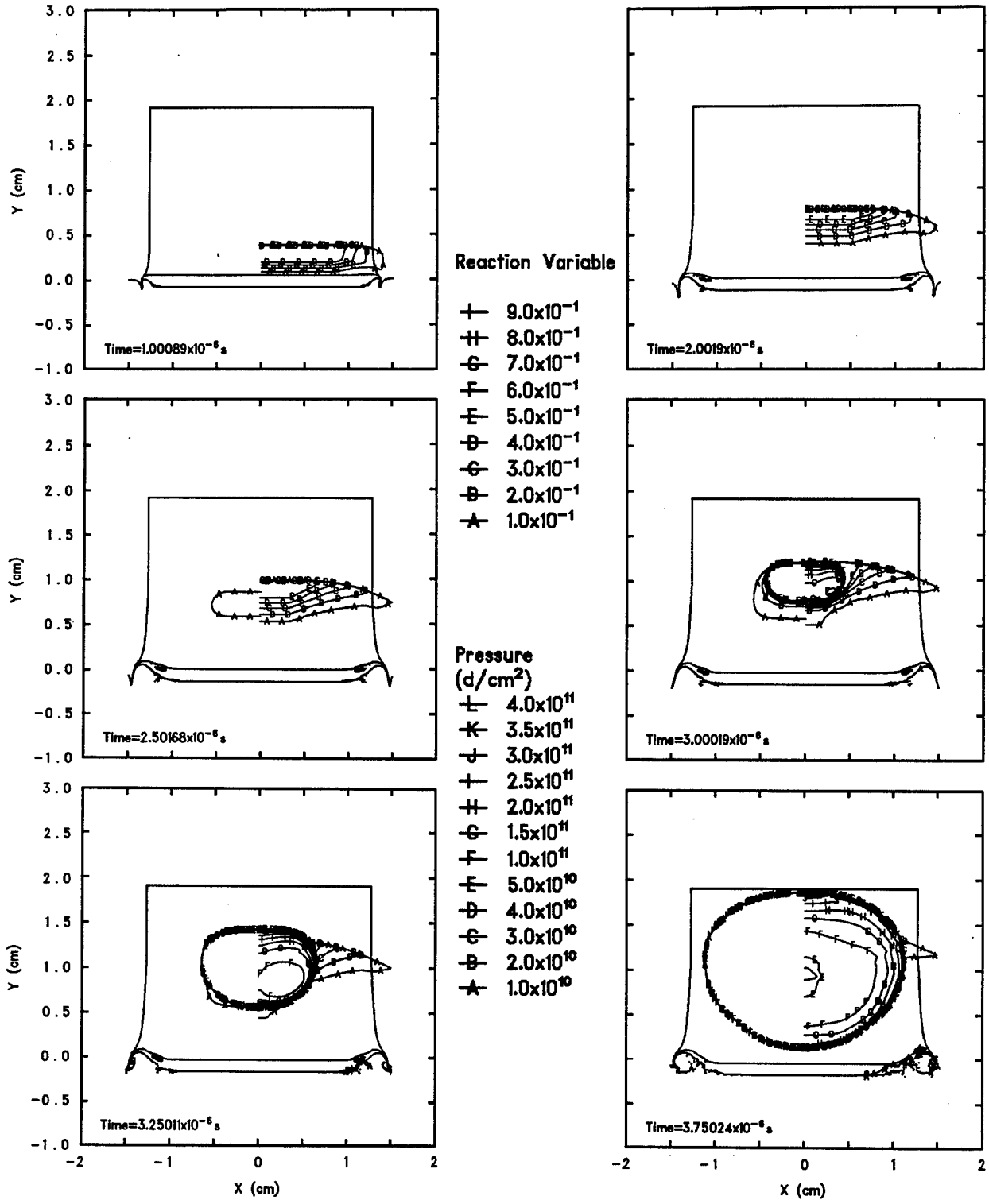

Figure 5. Sequence of Pressure and Reaction Variable Contour Plots for the 1.5-km/s Impact of a 1.27-mm-Thick Mylar Flyer Against a PBX-9404 Charge.

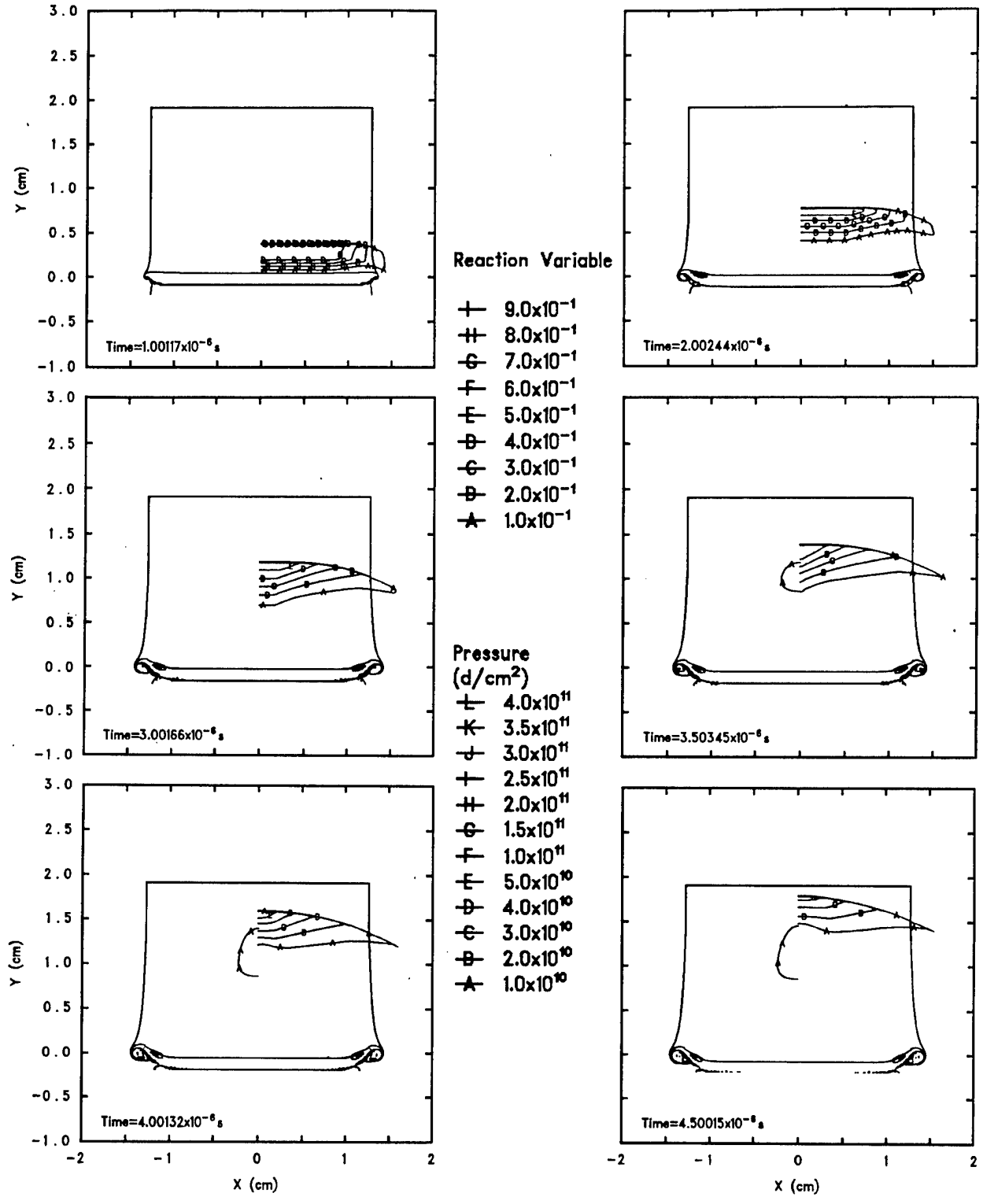

Figure 6. Sequence of Pressure and Reaction Variable Contour Plots for the 1.4-km/s Impact of a 1.27-mm-Thick Mylar Flyer Against a PBX-9404 Charge.

result. The CTH/HVRB critical velocity predictions are compared with the experiments and with Forest Fire predictions in Figure 7. The experimental results are fit well by a straight line in a plot of the logarithm of the flyer velocity versus the logarithm of the flyer thickness. While HVRB performs somewhat better than Forest Fire (which grossly overestimates the sensitivity of the explosive), it still underestimates the sensitivity considerably.

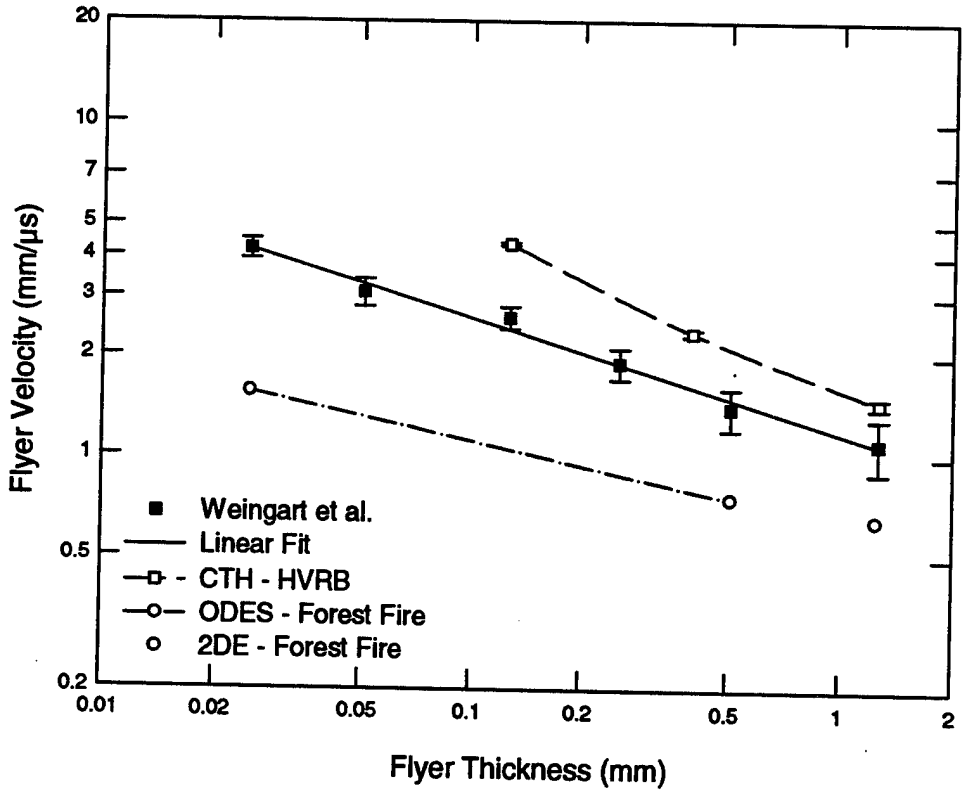

Figure 7. Comparison of HVRB and Forest Fire Predictions With Experimental Data for the Initiation of PBX-9404 Charges by the Impact of Thin Mylar Flyers.

6. Projectile-Impact Initiation of PBX-9404

The initiation of explosives due to projectile impact has been the subject of extensive experimental research. In this case, initiation is influenced by rarefactions emanating from the outer surface of the projectile that reduce reaction rates and attenuate impact shock waves. A study by

Bahl, Vantine, and Weingart (1981) produced critical velocities for impact of flat- and round-tipped cylindrical steel projectiles against bare and tantalum-covered PBX-9404 charges. The cover plates in these experiments were either 2- or 6-mm thick. The results of this study and our modified Jacobs-Roslund fits to the data are summarized in the appendix.

We made axisymmetric simulations of some of these experiments, representing the flat-tipped projectiles as right circular cylinders with unit length-to-diameter ratios and adding hemispheres to the leading edges to produce round-tipped projectiles. We maintained a fixed relationship between the projectile and the target, keeping the target diameter and depth equal to five times the projectile diameter. The computational zoning was varied with the projectile diameter: 0.1-mm, 0.2-mm, or 0.5-mm square zones were selected as appropriate.

In order to limit the number of computations, we considered only two projectile diameters (near the upper and lower end of the experimental range) for each of the three target configurations. We varied the projectile-impact velocity in order to determine critical values for initiation. Typical sequences of contour plots are shown in Figures 8–15.

Figure 8 shows a sequence of pressure and reaction variable contour plots for initiation of a bare PBX-9404 target by the impact of a 16-mm-diameter flat-tipped projectile at 0.60 mm/μs. This near-critical impact produces an initial shock pressure of about 3.9 GPa. In this case, the impact shock propagates approximately 8.3 mm into the target as a planar wave (i.e., without attenuation at the axis) before transitioning to detonation. This distance of run to detonation is less than 10% longer than that associated with the computed Pop plot, indicating minimal influence of the rarefaction on the reaction zone. When the impact velocity of the same projectile is reduced to 0.55 mm/μs, detonation fails to initiate in the same target, as shown in the sequence of pressure and reaction variable contour plots of Figure 9.

Results obtained with the projectile diameter reduced to 2 mm are shown in Figure 10. In this case, a near-critical 1.5-mm/μs impact produces an initial shock pressure of about 13.7 GPA, leading

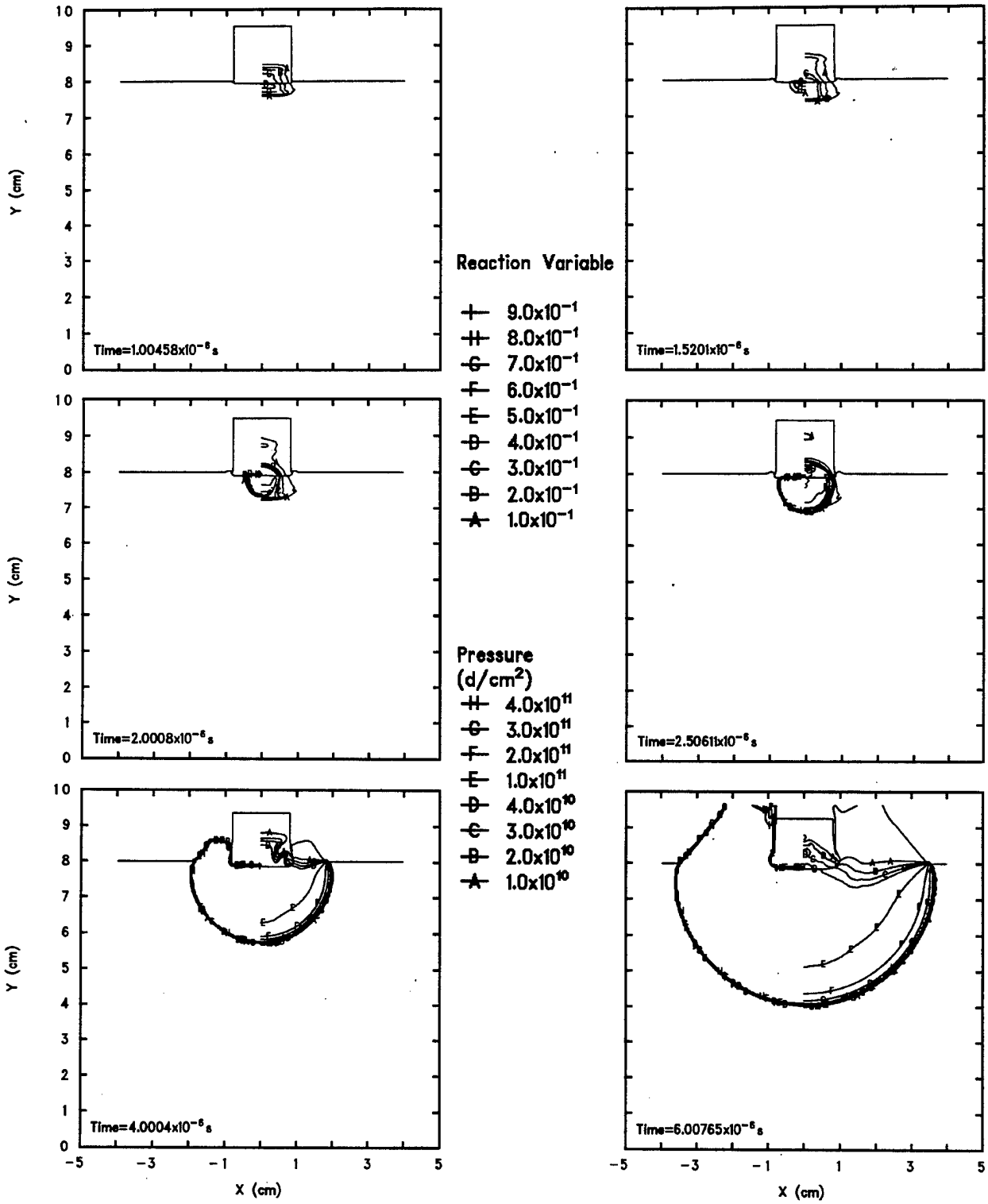

Figure 8. Sequence of Pressure and Reaction Variable Contour Plots Showing Initiation of a Bare PBX-9404 Target by the Impact of a 16-mm-Diameter Flat-Tipped Steel Projectile at 0.60 mm/μs.

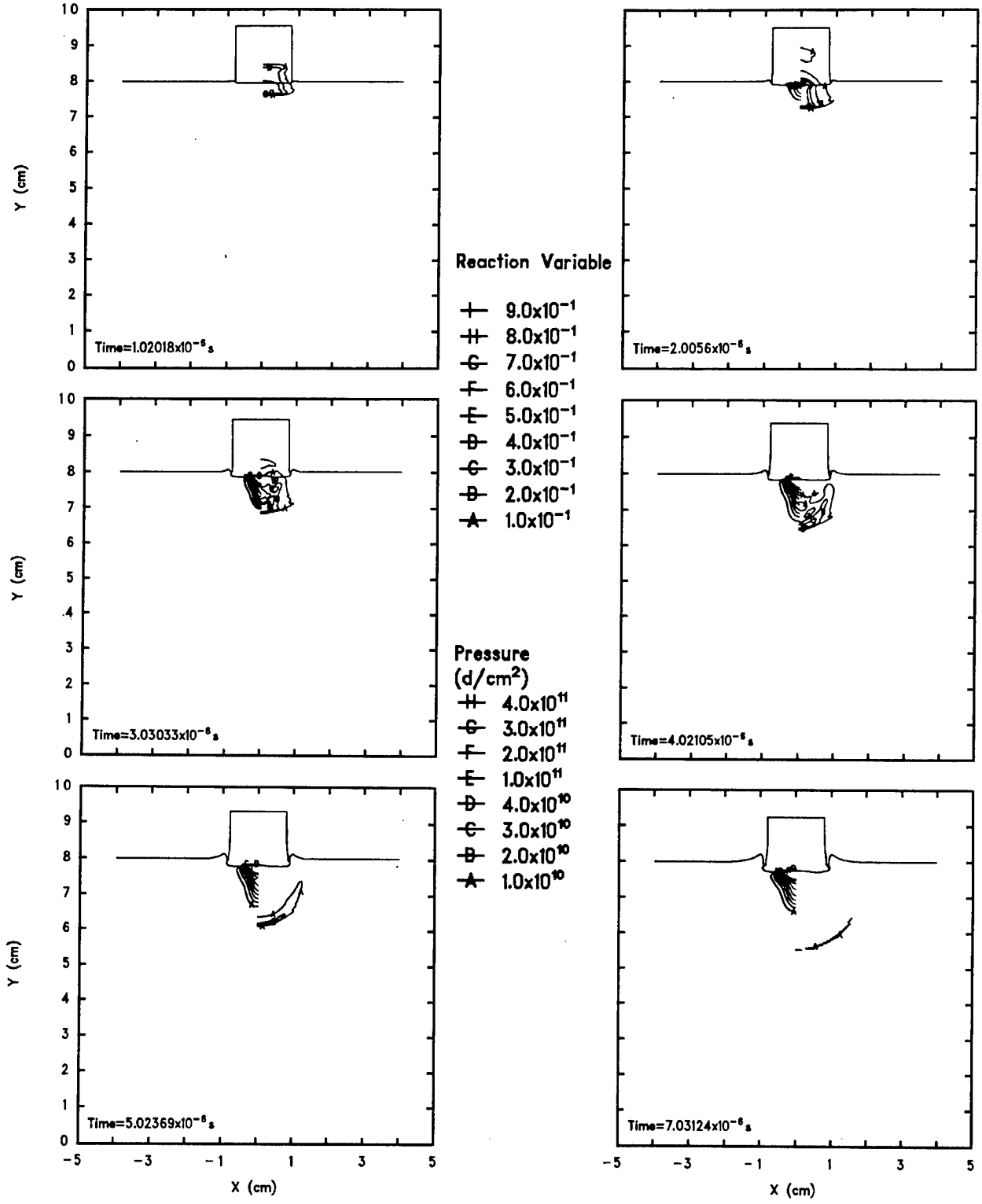

Figure 9. Sequence of Pressure and Reaction Variable Contour Plots Showing Initiation Failure in a Bare PBX-9404 Target Following Impact by a 16-mm-Diameter Flat-Tipped Steel Projectile at 0.55 mm/μs.

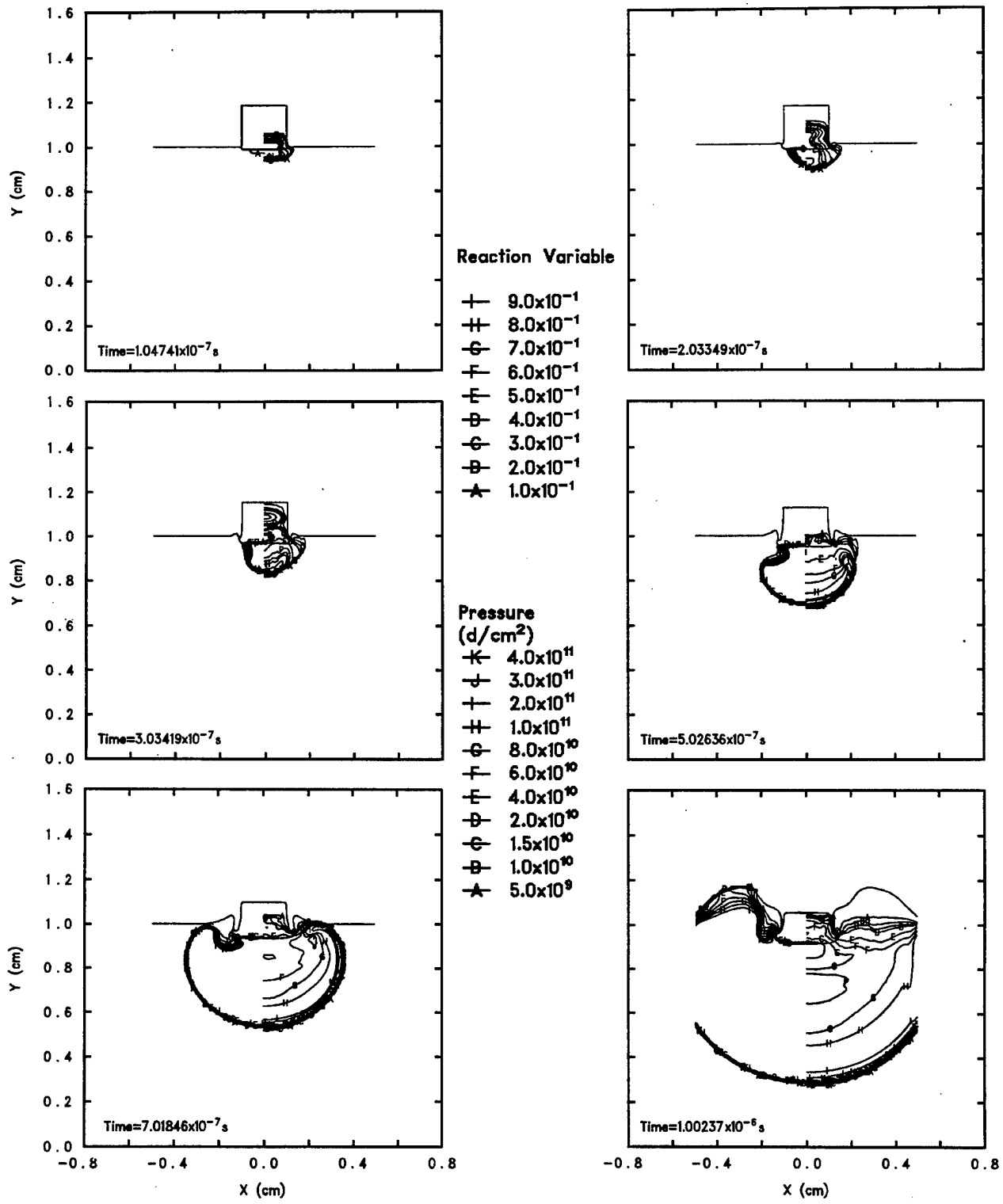

Figure 10. Sequence of Pressure and Reaction Variable Contour Plots Showing Initiation of a Bare PBX-9404 Target by the Impact of a 2-mm-Diameter Flat-Tipped Steel Projectile at 1.5 mm/μs.

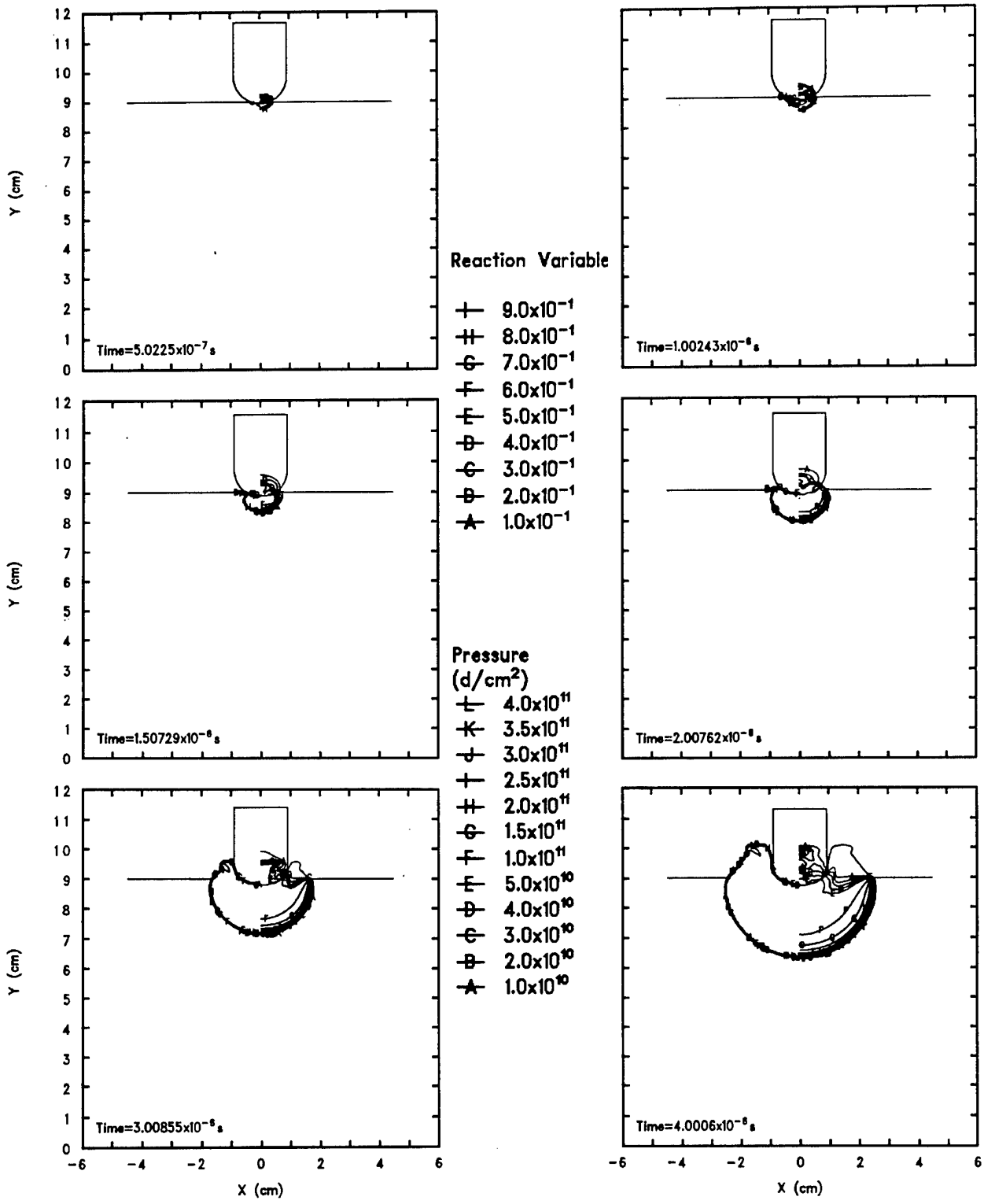

Figure 11. Sequence of Pressure and Reaction Variable Contour Plots Showing Initiation of a Bare PBX-9404 Target by the Impact of an 18-mm-Diameter Round-Tipped Steel Projectile at 1.0 mm/μs.

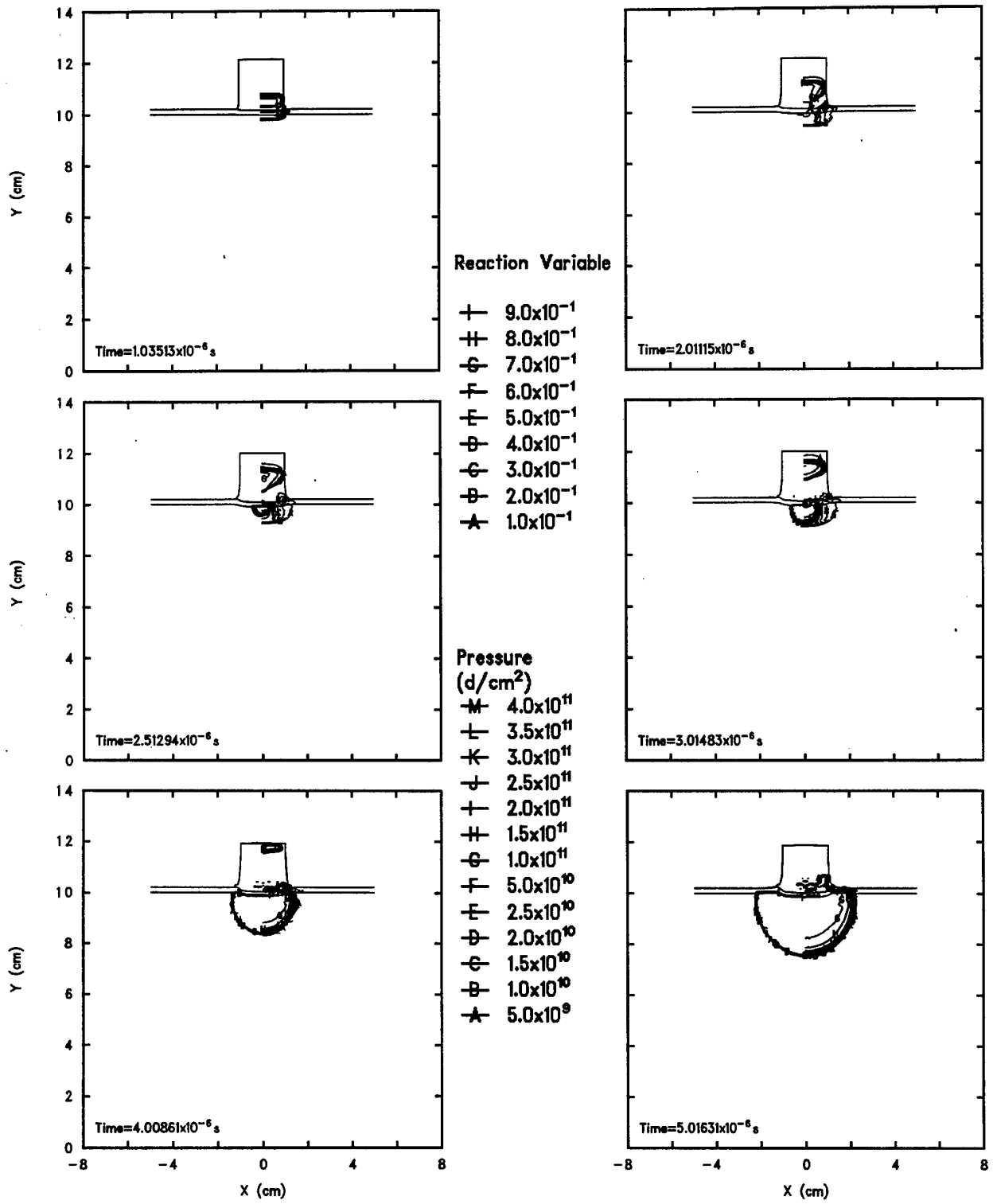

Figure 12. Sequence of Pressure and Reaction Variable Contour Plots Showing the Initiation of a PBX-9404 Target With a 2-mm-Thick Tantalum Cover by the Impact of a 20-mm-Diameter Flat-Tipped Steel Projectile at 0.7 mm/μs.

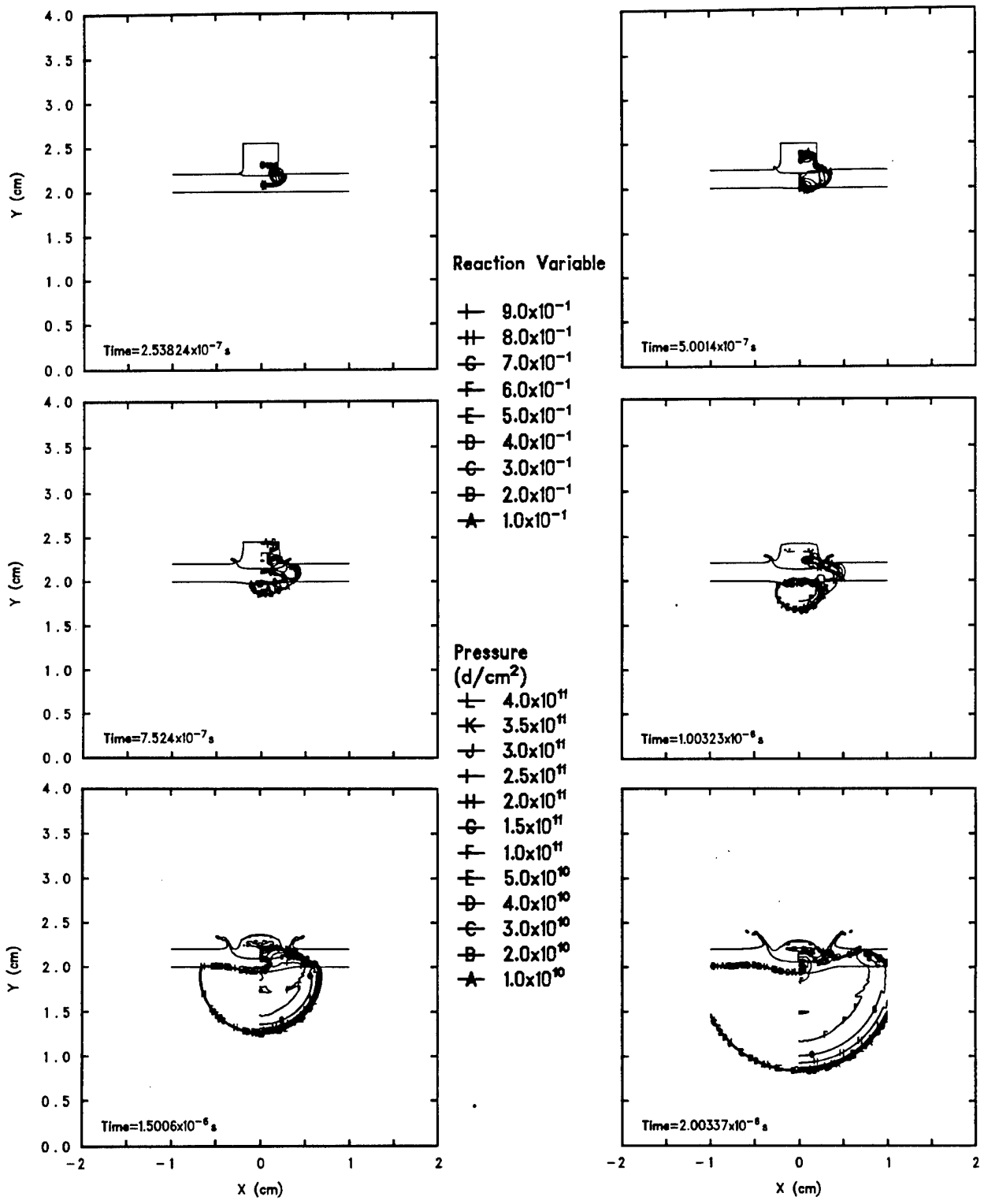

Figure 13. Sequence of Pressure and Reaction Variable Contour Plots Showing the Initiation of a PBX-9404 Target With a 2-mm-Thick Tantalum Cover by the Impact of a 4-mm-Diameter Flat-Tipped Steel Projectile at 2.0 mm/μs.

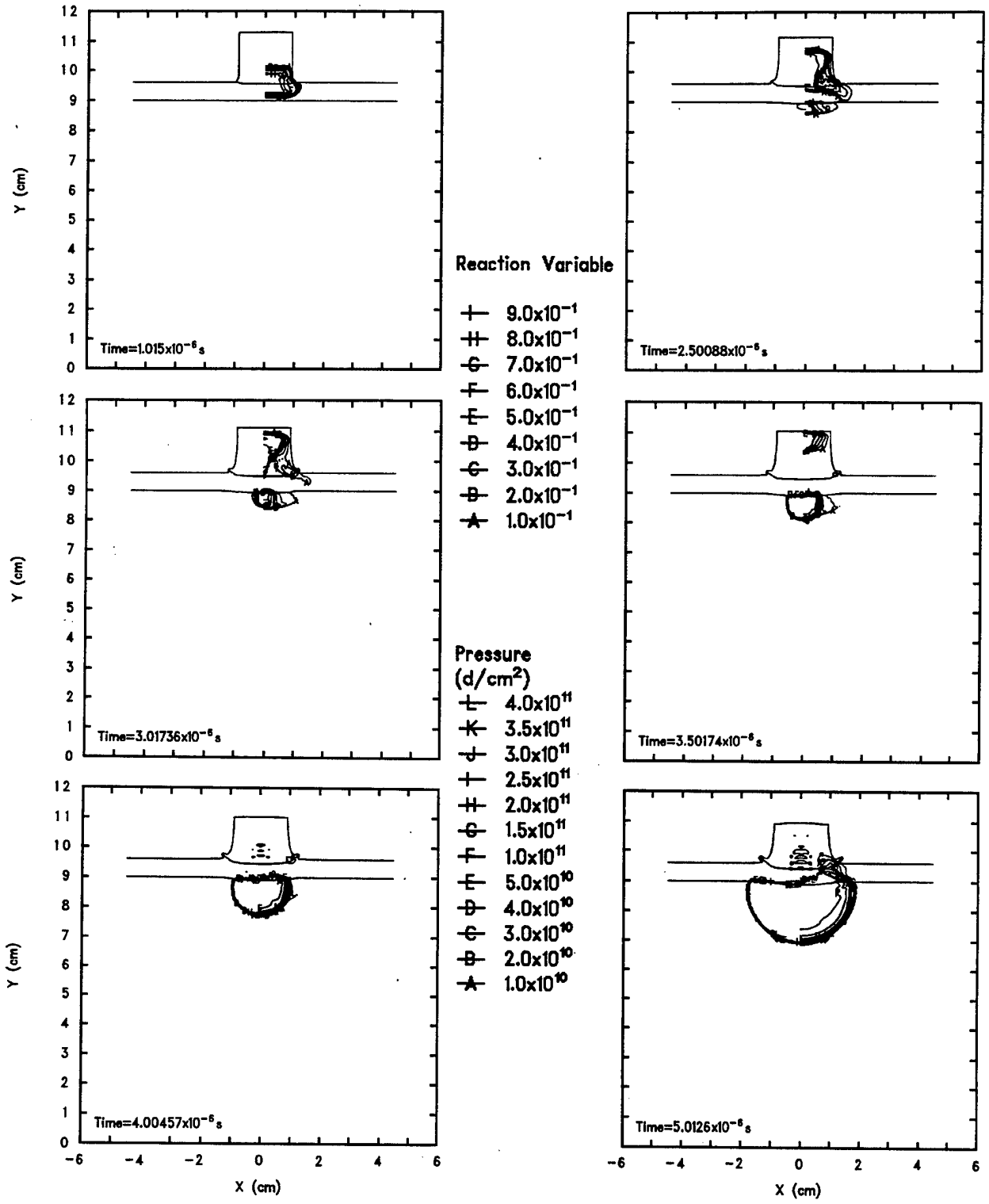

Figure 14. Sequence of Pressure and Reaction Variable Contour Plots Showing the Initiation of a PBX-9404 Target With a 6-mm-Thick Tantalum Cover by the Impact of an 18-mm-Diameter Flat-Tipped Steel Projectile at 1.0 mm/μs.

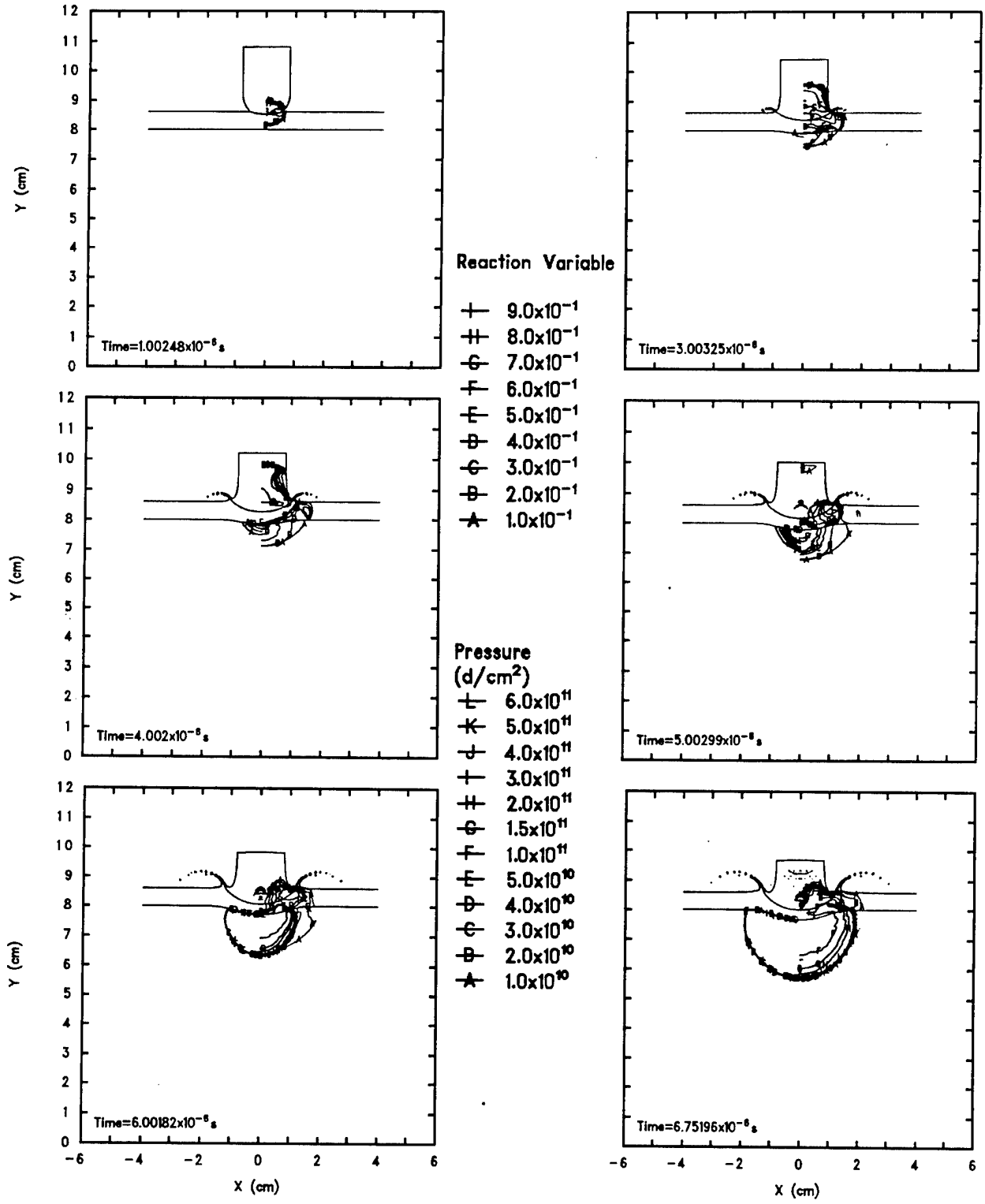

Figure 15. Sequence of Pressure and Reaction Variable Contour Plots Showing the Initiation of a PBX-9404 Target With a 6-mm-Thick Tantalum Cover by the Impact of a 16-mm-Diameter Round-Tipped Steel Projectile at 2.0 mm/μs.

to detonation. The run to detonation is about 1.5 mm, or nearly 50% greater than that associated with the Pop plot. The influence of the rarefaction on the reaction zone is significant.

With round-tipped projectiles, rarefactions enter the reaction zone immediately after impact, leading to higher critical velocities. Figure 11 shows a sequence of pressure and reaction variable contour plots for initiation of a bare target by the impact of an 18-mm-diameter flat-tipped projectile at 1.0 mm/μs. The initial pressure is about 7.8 GPa, and the run to detonation of about 6.0 mm is more than twice the Pop plot value.

The effect of a cover plate is to allow attenuation of the impact shock wave by the overtaking rarefaction prior to its entry into the explosive target, again, leading to higher critical velocities. If the ratio of the cover thickness to the projectile diameter is small enough, the central portion of the shock wave produced by the impact of a flat-tipped projectile will remain planar and unattenuated as it enters the explosive. This is the case for a 20-mm-diameter flat-tipped projectile and a 2-mm-thick tantalum cover. Results obtained with a projectile velocity of 0.7 mm/μs are shown in Figure 12. Initiation occurs within the planar region with a run to detonation comparable to that of the Pop plot.

With a small diameter projectile, or thick cover plate, the planar region of the impact shock may be totally attenuated within the cover. For example, when the projectile diameter is reduced to 4 mm with the same cover plate, an impact velocity of 2.0 mm/μs or greater is required to produce initiation. Results are shown in Figure 13. In this case, the run to detonation is longer than that associated with the Pop plot. Similar results are obtained in the case of a 18-mm-diameter flat-tipped projectile and a 6-mm-thick tantalum cover. With an impact velocity of 1.0 mm/μs, most of the planar region of the impact shock is attenuated within the cover as shown in Figure 14.

When the effects of the cover plate are combined with those of a round tip, even higher projectile velocities are required to produce detonation. Results for a 16-mm-diameter projectile with a velocity of 2.0 mm/μs impacting a 6-mm-thick cover plate are shown in Figure 15.

Critical velocities are plotted as functions of projectile diameter in Figures 16–20. The fits to experimental data are shown as solid lines bounded by filled symbols, while the computational results are plotted as open symbols connected by dashed lines. The results for bare explosive show excellent agreement with experiment for both flat- and round-tipped projectiles, as illustrated in Figure 16. With a 2-mm tantalum cover, the agreement is nearly as good, as shown in Figure 17. With a 6-mm tantalum cover, the agreement deteriorates for flat-tipped projectiles while remaining adequate in the case of round-tipped projectiles, as shown in Figure 18. The same data are plotted again in Figures 19 and 20, which show the trends with increasing target cover for each projectile tip shape.

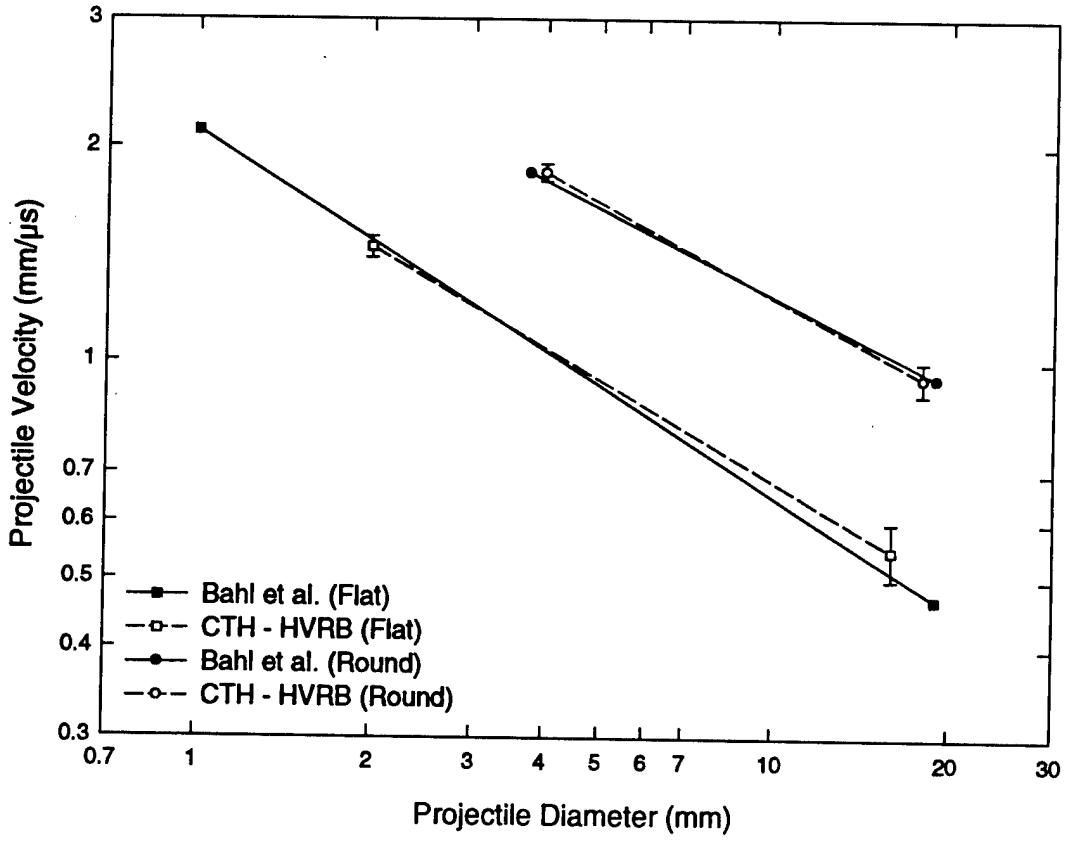

Figure 16. Comparison of HVRB Predictions With Experimental Data for the Critical Impact Velocity as a Function of the Diameter of Cylindrical Steel Projectiles Against Bare PBX-9404 Charges.

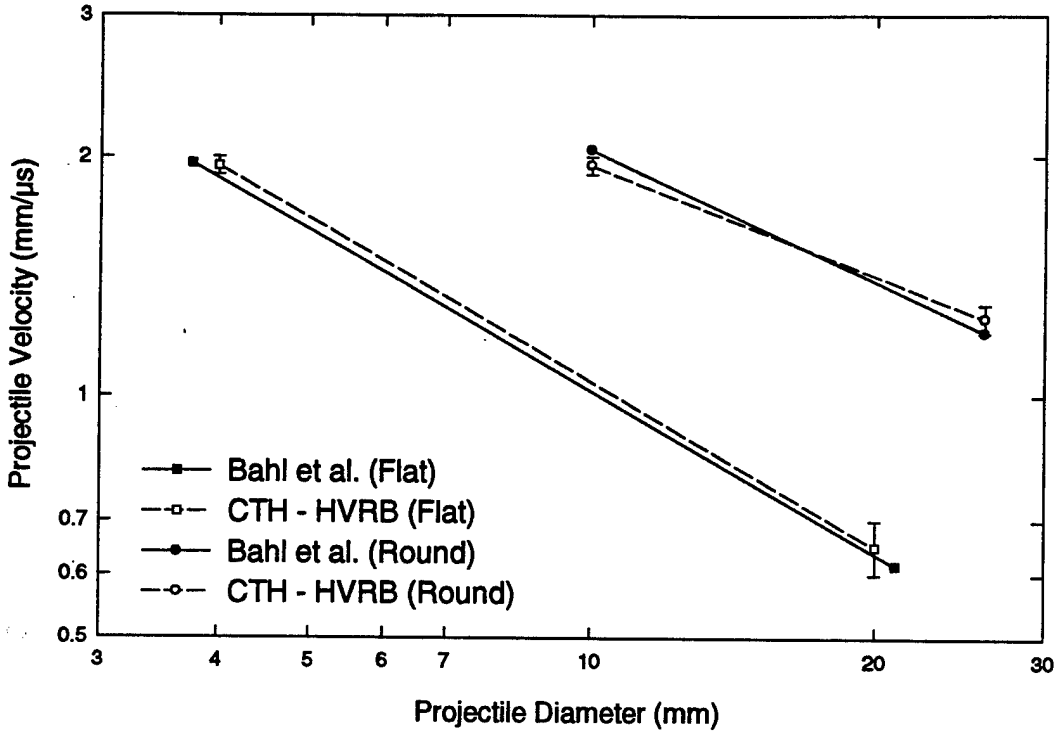

Figure 17. Comparison of HVRB Predictions With Experimental Data for the Critical Impact Velocity as a Function of the Diameter of Cylindrical Steel Projectiles Against 2-mm-Thick Tantalum-Covered PBX-9404 Charges.

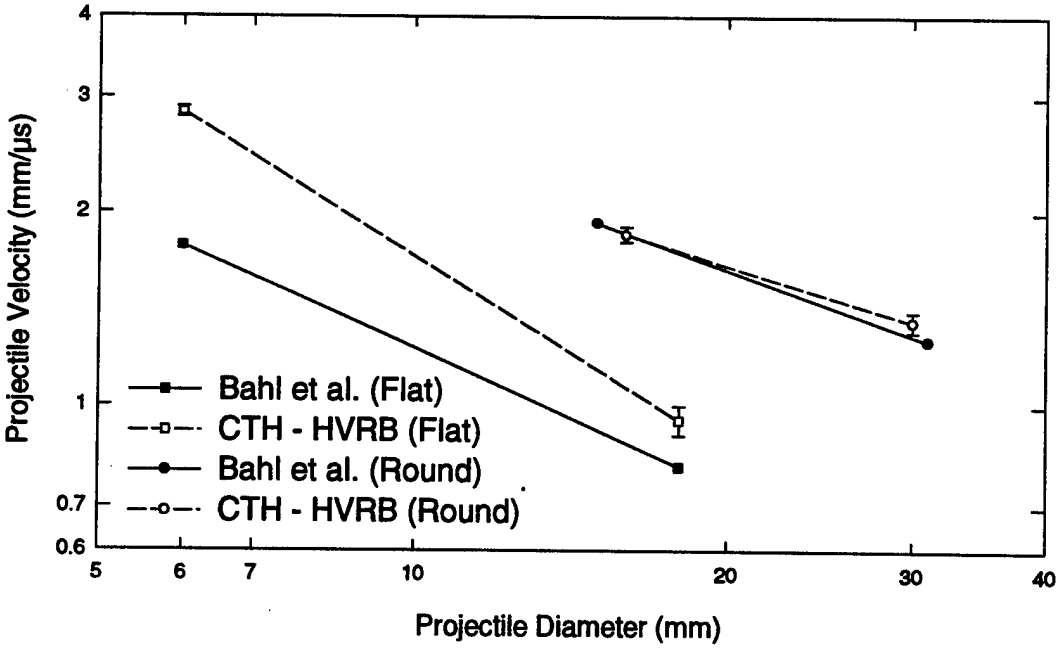

Figure 18. Comparison of HVRB Predictions With Experimental Data for the Critical Impact Velocity as a Function of the Diameter of Cylindrical Steel Projectiles Against 6-mm-Thick Tantalum-Covered PBX-9404 Charges.

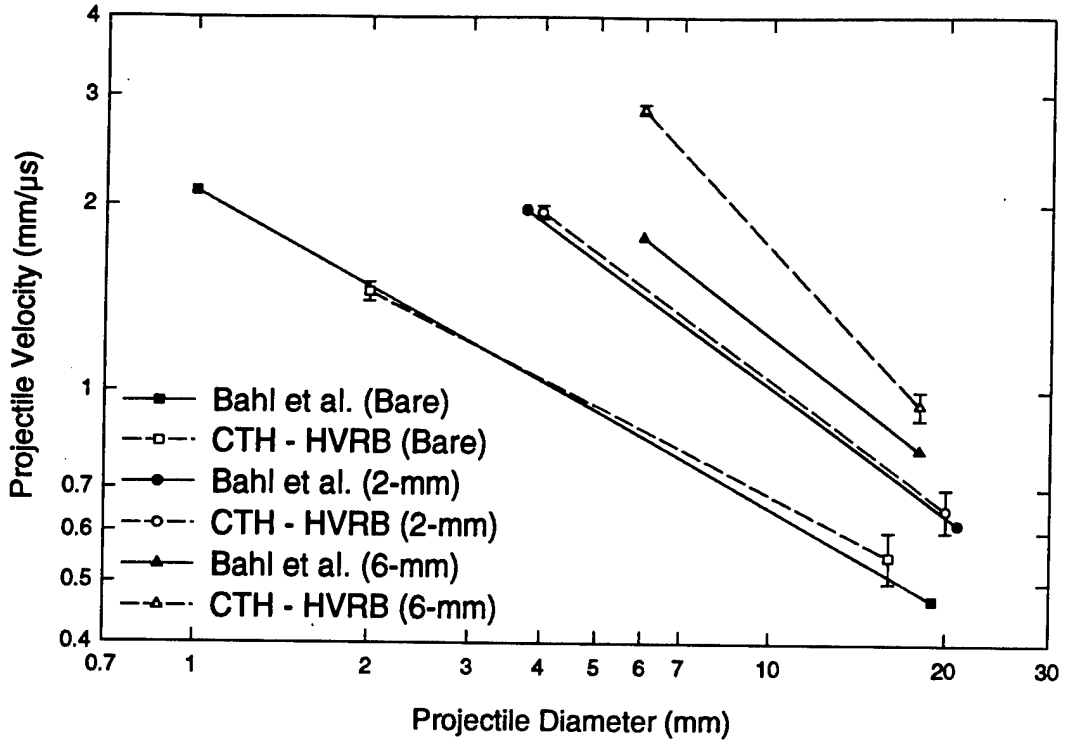

Figure 19. Comparison of HVRB Predictions With Experimental Data for the Critical Impact Velocity as a Function of the Diameter of Flat-Tipped Cylindrical Steel Projectiles Against Bare and Tantalum-Covered PBX-9404 Charges.

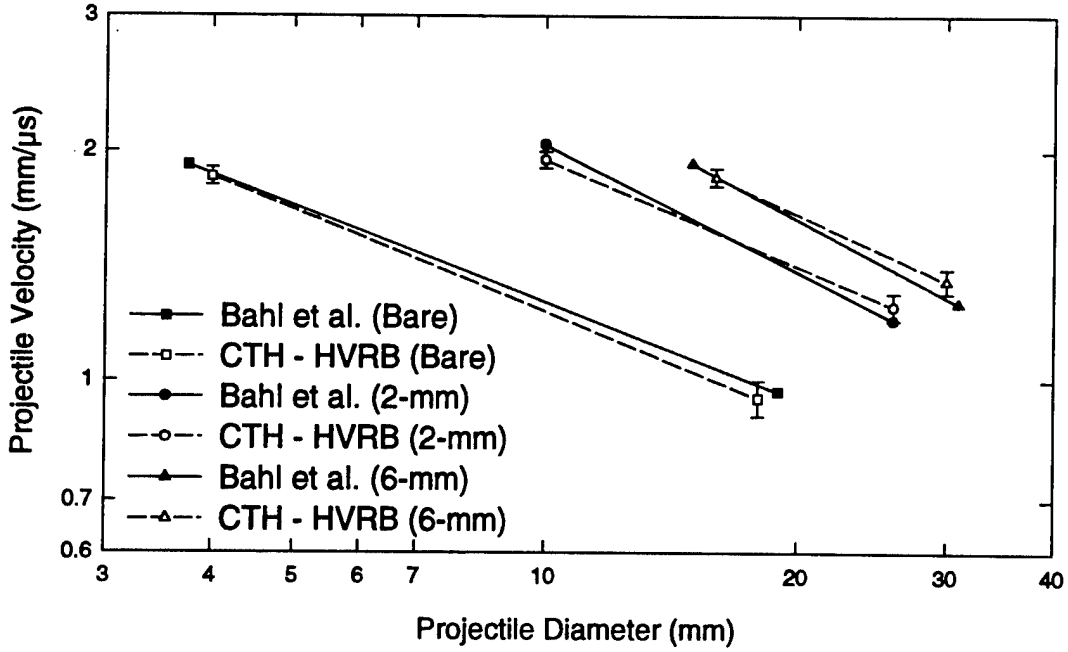

Figure 20. Comparison of HVRB Predictions With Experimental Data for the Critical Impact Velocity as a Function of the Diameter of Round-Tipped Cylindrical Steel Projectiles Against Bare and Tantalum-Covered PBX-9404 Charges.

7. Detonation Failure in Composition B Charges

It is well known that explosive charges can only sustain detonation when their lateral dimensions are sufficiently large. When this condition is not met, incipient detonations fail as a result of the effects of rarefactions that encroach upon their reaction zones. Thus, for a particular explosive, a failure diameter (or radius) may be determined for cylindrical charges, and a failure thickness may be determined for laminar charges. The phenomenon, which is of interest in its own right, has consequences for initiation of explosives by small projectiles such as shaped-charge jets (Chick et al. 1985, 1989; Starkenberg, Lawrence, and Dorsey 1994) and affects the ability of propagating detonations to turn corners in explosive charges.

Experimental data describing the failure diameter (Campbell and Engelke 1976; Dobratz 1985) and thickness (Urizar 1978; Gibbs and Popolato 1980) of several explosives are presented in Table 1. The last column of the table gives the ratio of the failure radius to the failure thickness. While the ratio varies between 0.64 and 1.21, in most cases, it lies very close to unity. Since these experiments were conducted by different researchers at different times, the explosives may not be identical. In fact, only Composition A-3 (for which a ratio of 0.96 applies) appears to have the same formulation and density in both experiments. Thus, the data are generally consistent with the hypothesis that the failure thickness and radius are equal.

Table 1. Experimental Failure Thickness and Radius for Selected Explosives

Explosive	Density (g/cm^3)	Failure Thickness (mm)	Explosive	Density (g/cm^3)	Failure Radius (mm)	Radius/ Thickness (mm/mm)
PBX 9404	1.83	0.92	PBX 9404	1.85	0.59	0.64
Comp. A-3	1.63	1.14	Comp. A-3	1.63	1.10	0.96
Cyclotol 75/25	1.75	3.02	Cyclotol 77/23	1.74	3.00	0.99
Comp. B-3	1.72	1.88	Comp. B-3	—	2.00	1.06
Octol 75/25	1.79	2.86	Octol 75/25	1.81	3.20	1.12
Pentolite	1.70	2.78	Pentolite	—	3.35	1.21

The reaction zone for fully developed detonations is on the order of a millimeter for Composition B and is not well resolved in most computations. Such lack of computational resolution affects the accuracy of detonation failure predictions. However, sufficiently fine zoning should produce accurate solutions that are independent of zone size. Mader (1979) has reported accurate predictions of failure diameter in several explosives using the Forest Fire model in the 2DL and 2DE codes. Lundstrom (1993) has produced less successful predictions of the failure diameter of Composition B using his modified version of Forest Fire in the SMERF code. He observed rapid increases in failure diameter with zone size at the smallest zone sizes he used. More recently, we obtained accurate predictions of the failure radius and thickness of Composition B that are independent of computational zone size using 2DE and the original version of Forest Fire (Starkenberg and Dorsey 1994). These indicate that the failure thickness of an explosive is generally equal to its failure radius.

In order to obtain an understanding of the utility of HVRB in predicting detonation failure, we made both axisymmetric and plane-strain computations to predict the failure radius and thickness of Composition B. The simulation consists of Composition B booster and main charges surrounded by air. Initiation is achieved by means of programmed burn detonation in the booster charge. Reaction in the main charge is described using HVRB. We made use of the CTH velocity addition feature to subtract an axial velocity approximately equal to the detonation velocity throughout the mesh at a specified time. This serves to freeze a detonation after it has propagated a desired distance (in our case, approximately halfway through the mesh). When the detonation fails, the decaying wave is swept off the bottom of the mesh. We modified an input template suggested by Kerley (1995) for the purpose of initializing the computations. As the charge radius or thickness is varied, the dimensions of the computational mesh, the length of the booster charge, and the time for the velocity addition are varied proportionally with a fixed zone size.

Typical sequences of contour plots for failure-radius computations are shown in Figures 21 and 22. For these computations, we used zone sizes ranging from 0.04- to 0.20-mm square. Figure 21 shows detonation propagation through 7.0 μs in a 2.04-mm radius charge using a zone size of 0.12 mm. A velocity of 7.65 mm/μs is subtracted from the grid at 1.1 μs. After this, the detonation

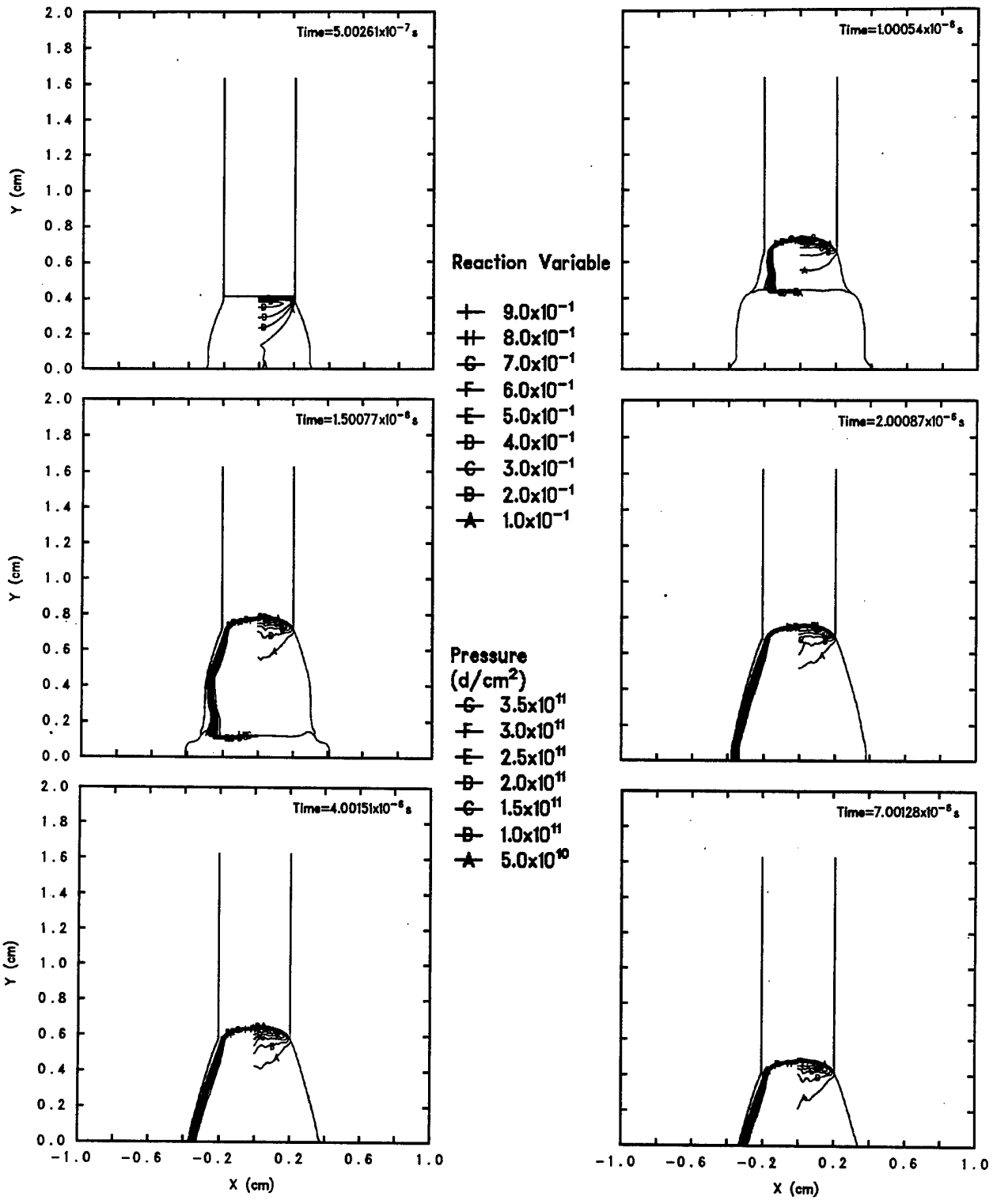

Figure 21. Sequence of Pressure and Reaction Variable Contour Plots for Detonation Propagation in a 2.04-mm-Radius Cylindrical Composition B Charge.

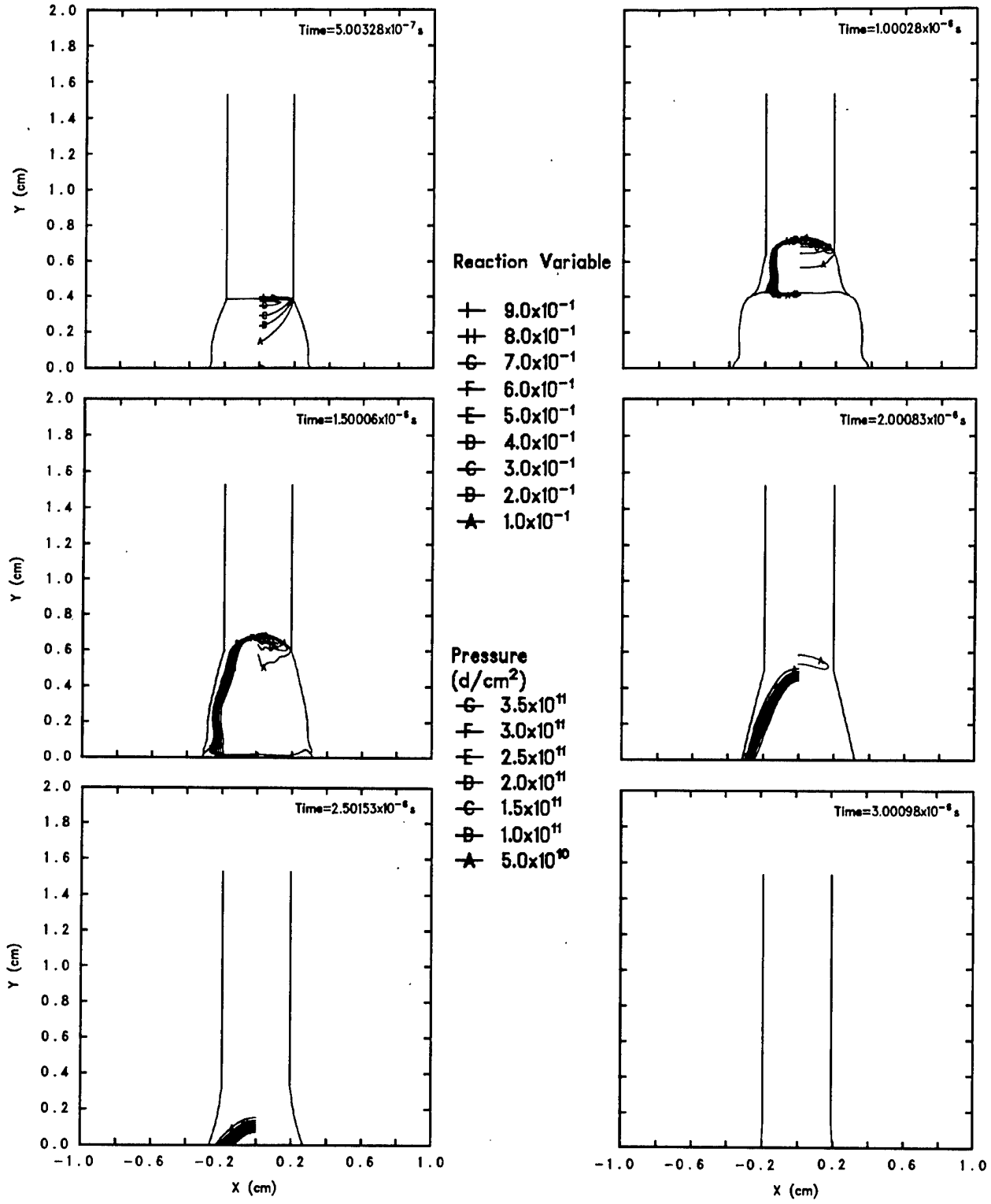

Figure 22. Sequence of Pressure and Reaction Variable Contour Plots for Detonation Failure in a 1.92-mm-Radius Cylindrical Composition B Charge.

front drifts slowly downward in the grid because its propagation velocity is a little lower than the subtracted velocity. In a similar computation with a 1.92-mm radius charge, the detonation failed after about 1.5 μs, as shown in Figure 22. All activity is swept off the mesh by 3.0 μs.

We have plotted the CTH failure-radius predictions, along with the results we obtained with 2DE, as well as those of Lundstrom, as functions of zone dimension in Figure 23. While our 2DE computations converged nicely with decreasing zone size, Lundstrom did not observe such convergence in his computations, which exhibit a minimum in predicted failure radius. CTH also produces solutions that appear to diverge with decreasing zone size, although not as rapidly as Lundstrom's. The apparent divergence does not imply that the solutions never converge, only that they do not converge for zone sizes that are practical to use. The failure radius predicted with CTH also exhibits a minimum, near which the solution is most stable (least sensitive to variations in zone size), at a zone dimension of 0.12 mm. This minimum value agrees well with the experimental failure radius (Campbell and Engelke 1976; Dobratz 1985). The CTH most stable zone size is somewhat larger than that determined by Lundstrom and the zone size required for convergence with 2DE. The most stable zone size can be applied to other configurations in which detonation failure is an issue (in particular, to shaped-charge jet attack).

For the failure thickness computations, we used zone sizes ranging from 0.01- to 0.20-mm square. Results obtained are plotted in Figure 24. In this case, the most stable zone size is about 0.02 mm, much smaller than in the failure-radius case. The associated failure-thickness prediction is a little larger than the experimental value (Urizar 1978; Gibbs and Popolato 1980). However, the experimental method is indirect and renders the latter value suspect. Agreement with the experimental failure radius (which may more accurately represent the failure thickness) is better.

8. Summary and Conclusions

We exercised the HVRB model in the CTH code, simulating a number of common explosive sensitivity experiments, including sustained- and pulsed-shock initiation, projectile-impact initiation, and detonation failure.

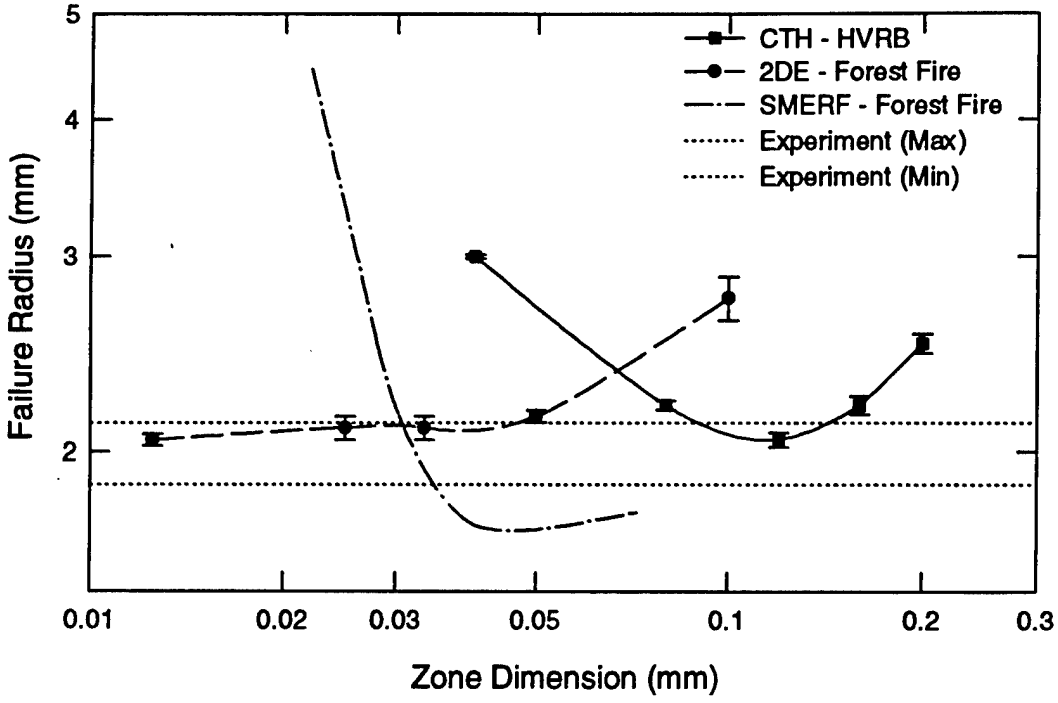

Figure 23. Comparison of HVRB and Forest Fire Predictions for Composition B Failure Radius as a Function of the Computational Zone Size.

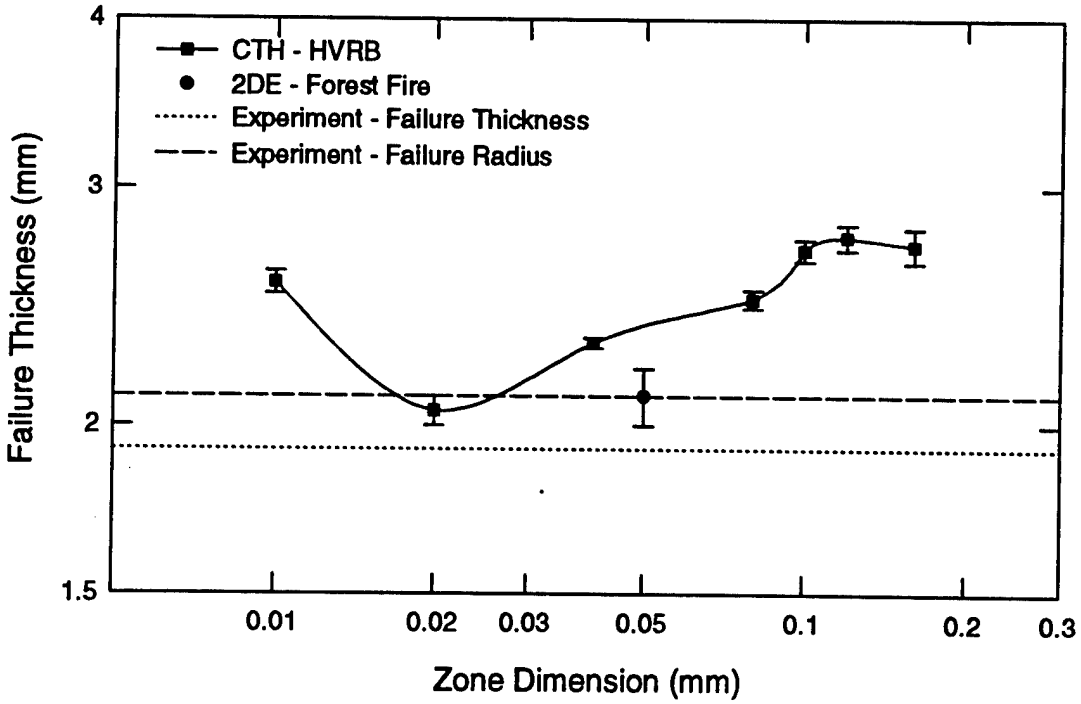

Figure 24. HVRB Predictions for Composition B Failure Thickness as a Function of the Computational Zone Size.

Predictions of sustained-shock initiation are accurate in accordance with the calibration of the model. Predictions of pulsed-shock initiation are only somewhat more accurate than those achieved previously using Forest Fire.

Predictions of projectile-impact initiation are much better. The results for bare explosive show excellent agreement with experiment for both flat- and round-tipped projectiles. With a 2-mm tantalum cover, the agreement is nearly as good. With a 6-mm tantalum cover, the agreement deteriorates for flat-tipped projectiles, while remaining adequate in the case of round-tipped projectiles.

The failure radius predicted with CTH exhibits a minimum (near which the solution is most stable) as a function of zone dimension, but does not appear to converge. This minimum value agrees well with experiment. Results for failure thickness are similar. The most stable value is a little larger than the experimental failure thickness and roughly equal to the experimental failure radius.

Difficulties associated with resolution of the reaction zone may limit the accuracy of predictions in problems where large amounts of reaction occur over short distances. Cognizance of these difficulties is important in conducting simulations of detonation failure, corner turning, and initiation by projectiles having diameters smaller than the explosive's failure diameter.

INTENTIONALLY LEFT BLANK.

9. References

Baer, M. R., and J. W. Nunziato. "Compressive Combustion of Granular Materials Induced by Low-Velocity Impact." *Proceedings of the Ninth Symposium (International) on Detonation,* pp. 604–617, August 1989.

Bahl, K. L., H. C. Vantine, and R. C. Weingart. "The Shock Initiation of Bare and Covered Explosives by Projectile Impact." *Proceedings of the Seventh Symposium (International) on Detonation,* pp. 325–335, June 1981.

Campbell, A. W., and R. Engelke. "The Diameter Effect in High-Density Heterogeneous Explosives." *Proceedings of the Sixth Symposium (International) on Detonation,* pp. 642–652, 1976.

Chick, M. C., I. B. McIntyre, and R. B. Frey. "The Jet Initiation of Solid Explosive." *Proceedings of the Eighth Symposium (International) on Detonation,* pp. 377–382, July 1985.

Chick, M. C., T. J. Bussell, R. B. Frey, and A. L. Bines. "Jet Initiation Mechanisms and Sensitivities of Covered Explosives." *Proceedings of the Ninth Symposium (International) on Detonation,* pp. 1404–1415, August 1989.

Dobratz, B. M. (ed.). *LLNL Explosives Handbook,* pp. 8–31, January 1985.

Gibbs, T. R., and A. Popolato (ed.). *LASL Explosive Property Data,* pp. 289–290, 1980.

Hertel, E. S. Jr., R. L. Bell, M. G. Elrick, A. V. Farnsworth, G. I. Kerley, J. M. McGlaun, S. V. Petney, S. A. Silling, P. A. Taylor and, L. Yarrington. "CTH: A Software Family for Multi-Dimensional Shock Physics Analysis." *Proceedings of the 19th International Symposium on Shock Waves,* vol. 1, pp. 377–382, July 1993.

Johnson, J. N., P. K. Tang and C. A. Forest. "Shock Wave Initiation of Heterogeneous Reactive Solids." *Journal of Applied Physics,* vol. 57, no. 9, 1985.

Kerley, G. I. "CTH Equation of State Package: Porosity and Reactive Burn Models." SAND92-0553, Sandia National Laboratories, NM, April 1992.

Kerley, G. I. Personal communication. Albuquerque, NM, 1995.

Kershner, J. D., and C. L. Mader. "2DE, A Two-Dimensional Continuous Eulerian Hydrodynamic Code for Computing Multicomponent Reactive Hydrodynamic Problems." LA-4846, Los Alamos Scientific Laboratory, NM, 1972.

Lee, E. L., and C. M. Tarver. "Phenomenological Model of Shock Initiation in Heterogeneous Explosives." *Physics of Fluid,* vol. 23, no. 12, pp. 2362–2372, December 1980.

Lundstrom, E. A. "Evaluation of Forest Fire Burn Model of Reaction Kinetics of Heterogeneous Explosives." Naval Weapons Center Technical Publication 6898, Naval Weapons Center, CA, 1988.

Lundstrom. E. A. "A Numerical Study of Fragment Impact on Bare Explosive." *Proceedings of the 1993 JANNAF Propulsion Systems Hazards Subcommittee Meeting,* 1993.

Mader, C. L. "An Empirical Model of Heterogeneous Shock Initiation of 9404." Los Alamos Scientific Laboratory Report LA-4475, Los Alamos Scientific Laboratory, NM, 1970.

Mader, C. L., and C. A. Forest. "Two Dimensional Homogeneous and Heterogeneous Detonation Wave Propagation." Los Alamos Scientific Laboratory Report LA-6259, Los Alamos Scientific Laboratory, NM, 1976.

Mader, C. L. "Numerical Modeling of Detonation." University of California Press, Berkeley, 1979.

Menikoff, R. Personal communication. Los Alamos, NM, 1996.

Nutt, G. L., and L. M. Erickson. "Reactive Flow Lagrange Analysis in Plastic Bonded Explosives." *Journal of Energetic Materials,* vol. 2, pp. 263–292, 1984.

Ramsay, J. B., and A. Popolato. "Analysis of Shock Wave and Initiation Data for Solid Explosives." *Proceedings of the Fourth Symposium (International) on Detonation,* pp. 233–238, 1965.

Starkenberg, J. "A Model for the Initiation of Heterogeneous High Explosives Subject to General Compressive Loading." *Proceedings of the Ninth Symposium (International) on Detonation,* pp. 604–617, August 1989.

Starkenberg, J. "An Assessment of the Performance of the Original and Modified Versions of the Forest Fire Explosive Initiation Model." *Proceedings of the Tenth International Detonation Symposium,* p. 6, 1993.

Starkenberg, J., and T. M. Dorsey. "A Computational Study of Detonation Failure in Composition B and Cast TNT Charges." Technical Report, U.S. Army Research Laboratory, Aberdeen Proving Ground, MD, 1994.

Starkenberg, J., W. Lawrence, and T. M. Dorsey. "A Computational Study of the Effects of an Explosive's Failure Diameter on its Response to Shaped-Charge Jet Attack." *Proceedings of the 1994 JANNAF Propulsion Systems Hazards Subcommittee Meeting,* August 1994.

Tang, P. K., J. N. Johnson, and C. A. Forest. "Modeling Heterogeneous High Explosive Burn With an Explicit Hot-Spot Process." *Proceedings of the Eighth Symposium (International) on Detonation,* pp. 52–61, July 1985.

Urizar, M. J., S. W. Peterson, and L. C. Smith. "Detonation Sensitivity Tests." Los Alamos Scientific Laboratory Informal Report LA-7-93-MS, Los Alamos Scientific Laboratory, NM, April 1978.

Wackerle, J., R. L. Rabie, M. J. Ginsberg, and A. B. Anderson. "A Shock Initiation Study of PBX-9404." *Proceedings of the Symposium on High Dynamic Pressure,* August 1978.

Weingart, R. C., R. K. Jackson, C. A. Honodel, and R. S. Lee. "Shock Initiation of PBX-9404 By Electrically Driven Flyer Plates." *Propellants and Explosives,* vol. 5, pp. 158–162, 1980.

INTENTIONALLY LEFT BLANK.

Appendix:

Modified Jacobs-Roslund Fits to PBX-9404 Projectile-Impact Initiation Data

INTENTIONALLY LEFT BLANK.

The widely used Jacobs-Roslund formula giving the critical impact velocity for initiation of an explosive charge as a function of projectile diameter may be written

$$v_{crit} = \frac{A(1 + B)}{d^{1/2}} \left(1 + C\frac{h}{d}\right),$$

where d is the projectile diameter; h is the thickness of the plate covering the explosive charge; and A, B, and C are constants used to fit the equation to available data. In fact, there are only two independent constants, A(1 + B) and C. The constant B, which vanishes for flat-tipped projectiles, is a convenience used to account for the effect of projectile tip shape. The constant A is then calibrated using data for flat-tipped projectiles and bare explosive charges. The constant C is clearly associated with the effect of the cover plate.

Bahl, Vantine, and Weingart[1] produced an excellent set of data identifying initiation thresholds for bare and tantalum-covered PBX-9404 charges attacked by flat- and round-tipped projectiles. Liddiard and Roslund[2] have summarized the data (including that for PBX-9404) and provided fit constants for a number of explosives. Starting with the bare-charge data for flat-tipped projectiles, they identified pairs of data points near the threshold that include one go and one no-go. They then determined the midpoint of each pair by averaging the associated impact velocities and the inverse square roots of the associated projectile diameters. They then computed the constant A for each pair. Since the standard deviation was small, they used the average value of A for the fit. Following a similar procedure using the round-tipped projectile data, they determined values for the constant B. Since B appeared to vary with projectile diameter, at least at larger diameters, they argued that this reflected a charge size effect in the experiments and that B should be determined from data for projectiles having diameters of 7 mm or less. Similar determinations of C, however, indicated that

---

[1] Bahl, K. L., H. C. Vantine, and R. C. Weingart. "The Shock Initiation of Bare and Covered Explosives by Projectile Impact." *Proceedings of the Ninth Symposium (International) on Detonation*, pp. 604–617, August 1985.

[2] Liddiard, T. P., and L. A. Roslund. "Projectile/Fragment Impact Sensitivity of Explosives." NSWC-TR89-184, Naval Surface Weapons Center, 1993.

it depends on tip shape and is not constant. The midpoint data used in this procedure are given in Tables A-1 and A-2.

Table A-1. Critical Velocities for Impact of Flat-Tipped Projectiles

Bare Charge		2-mm Tantalum Cover		6-mm Tantalum Cover	
d (mm)	v_{crit} (mm/μs)	d (mm)	v_{crit} (mm/μs)	d (mm)	v_{crit} (mm/μs)
1.13	2.070	3.684	1.840	6.20	1.93
1.28	1.910	3.724	1.940	7.90	1.50
1.49	1.620	3.913	1.740	10.00	1.26
2.20	1.380	3.968	1.840	15.01	0.95
3.14	1.130	4.675	1.605	18.00	0.84
3.68	1.085	5.656	1.420	—	—
7.73	0.745	7.631	1.130	—	—
8.70	0.695	8.858	1.040	—	—
12.76	0.575	12.986	0.840	—	—
17.73	0.500	20.291	0.650	—	—

Table A-2. Critical Velocities for Impact of Round-Tipped Projectiles

Bare Charge		2-mm Tantalum Cover		6-mm Tantalum Cover	
d (mm)	v_{crit} (mm/μs)	d (mm)	v_{crit} (mm/μs)	d (mm)	v_{crit} (mm/μs)
3.968	1.910	10.0	1.94	15.0	1.93
4.234	1.785	15.0	1.59	20.0	1.67
4.451	1.845	17.3	1.50	23.5	1.50
4.747	1.720	20.0	1.40	25.0	1.44
5.373	1.615	26.0	1.25	31.0	1.23
6.575	1.530	—	—	—	—
10.750	1.210	—	—	—	—
11.413	1.185	—	—	—	—
12.015	1.160	—	—	—	—
14.080	1.100	—	—	—	—
16.458	1.040	—	—	—	—
18.904	0.960	—	—	—	—

Using all of this data, we found that better fits could be obtained in the form

$$v_{crit} = \frac{A}{d^a}\left[1 + B\left(\frac{h}{d}\right)^b\right].$$

If a = 0.5 and b = 1.0, this is identical to the Jacobs-Roslund form. The constants we used, along with corresponding Jacobs-Roslund constants, are shown in Table A-3.

Table A-3. Critical Velocity Fitting Parameters

		A ($mm^{3/2}/\mu s$)	a	B	b
Flat	Present	2.109	0.51	1.098	0.45
	J-R	2.09	0.50	1.90	1.00
Round	Present	3.338	0.42	1.156	0.40
	J-R	3.78	0.50	0.630	1.00

INTENTIONALLY LEFT BLANK.

NO. OF COPIES ORGANIZATION

2 DEFENSE TECHNICAL INFORMATION CENTER
DTIC DDA
8725 JOHN J KINGMAN RD
STE 0944
FT BELVOIR VA 22060-6218

1 HQDA
DAMO FDQ
DENNIS SCHMIDT
400 ARMY PENTAGON
WASHINGTON DC 20310-0460

1 DPTY ASSIST SCY FOR R&T
SARD TT F MILTON
RM 3EA79 THE PENTAGON
WASHINGTON DC 20310-0103

1 OSD
OUSD(A&T)/ODDDR&E(R)
J LUPO
THE PENTAGON
WASHINGTON DC 20301-7100

1 CECOM
SP & TRRSTRL COMMCTN DIV
AMSEL RD ST MC M
H SOICHER
FT MONMOUTH NJ 07703-5203

1 PRIN DPTY FOR TCHNLGY HQ
US ARMY MATCOM
AMCDCG T
M FISETTE
5001 EISENHOWER AVE
ALEXANDRIA VA 22333-0001

1 DPTY CG FOR RDE HQ
US ARMY MATCOM
AMCRD
BG BEAUCHAMP
5001 EISENHOWER AVE
ALEXANDRIA VA 22333-0001

1 INST FOR ADVNCD TCHNLGY
THE UNIV OF TEXAS AT AUSTIN
PO BOX 202797
AUSTIN TX 78720-2797

NO. OF COPIES ORGANIZATION

1 GPS JOINT PROG OFC DIR
COL J CLAY
2435 VELA WAY STE 1613
LOS ANGELES AFB CA 90245-5500

1 ELECTRONIC SYS DIV DIR
CECOM RDEC
J NIEMELA
FT MONMOUTH NJ 07703

3 DARPA
L STOTTS
J PENNELLA
B KASPAR
3701 N FAIRFAX DR
ARLINGTON VA 22203-1714

1 US MILITARY ACADEMY
MATH SCI CTR OF EXCELLENCE
DEPT OF MATHEMATICAL SCI
MDN A MAJ DON ENGEN
THAYER HALL
WEST POINT NY 10996-1786

1 DIRECTOR
US ARMY RESEARCH LAB
AMSRL CS AL TP
2800 POWDER MILL RD
ADELPHI MD 20783-1145

1 DIRECTOR
US ARMY RESEARCH LAB
AMSRL CS AL TA
2800 POWDER MILL RD
ADELPHI MD 20783-1145

3 DIRECTOR
US ARMY RESEARCH LAB
AMSRL CI LL
2800 POWDER MILL RD
ADELPHI MD 20783-1145

ABERDEEN PROVING GROUND

4 DIR USARL
AMSRL CI LP (305)

NO. OF COPIES	ORGANIZATION
3	US ARMY ARDEC B D FISHBURN V M GOLD P LU PICATINNY ARSENAL NJ 07806-5000
3	NSWC R R BERNECKER H W SANDUSKY R M DOHERTY 101 STRAUSS AVE INDIAN HEAD MD 20640-5035
2	NAVAL EOD TECH DIV CODE 6021A R GOLD J DELANEY 2008 STUMP NECK ROAD INDIAN HEAD MD 20640-5070
1	USAF WL ARMAMENT DIRECTORATE ENERGETIC MTRL BRANCH J CORLEY 2306 PERIMETER RD STE 9 EGLIN AFB FL 32542-5910
1	USAF WL J G GLENN ARMAMENT DIRECTORATE EGLIN AFB FL 32542-5434
8	LANL B W ASAY C A FOREST J E KENNEDY E M KOBER R MENIKOFF P K TANG J B RAMSAY J WACKERLE LOS ALAMOS NM 87545
2	LANL J C DALLMAN P M HOWE PO BOX 1663 LOS ALAMOS NM 87545

NO. OF COPIES	ORGANIZATION
1	LANL W C DAVIS 693 46TH STREET LOS ALAMOS NM 87545
2	LLNL M J MURPHY C M TARVER PO BOX 808 LIVERMORE CA 94550
3	SNL M R BAER E S HERTEL R E SETCHELL PO BOX 5800 ALBUQUERQUE NM 87185-5800
1	VANDERBILT UNIVERSITY A M MELLOR BOX 1592 NASHVILLE TN 37235-1592
1	NM INSTITUTE OF MINING TECHNLGY L D LIBERSKY CAMPUS STATION SOCORRO NM 87801
1	KERLEY PUBLISHING SERVICES G I KERLEY PO BOX 13835 ALBUQUERQUE NM 87192-3835
1	GRYTING ENERGETICS SCIENCE CO H J GRYTING 7126 SHADOW RUN SAN ANTONIO TX 78250-3483
1	ATLANTIC RESEARCH CORP KENNETH GRAHAM 5945 WELLINGTON RD GAINSVILLE VA 22065-1699

NO. OF COPIES	ORGANIZATION
	ABERDEEN PROVING GROUND
15	DIR USARL AMSRL WM T W MORRISON AMSRL WM TB R FREY J WATSON V BOYLE W LAWRENCE R LOTTERO W HILLSTROM K BENJAMIN J DEHN E MCDOUGAL T DORSEY G RANDERS-PEHRSON L VANDEKIEFT P BAKER A FINNERTY

NO. OF COPIES	ORGANIZATION
1	DGA/CENTRE D'ETUDES DE GRAMAT DIDIER BERGUES GRAMAT, 46500 FRANCE
1	ICI EXPLOSIVES DAVID L. KENNEDY PO BOX 196 GEORGE BOOTH DRIVE NEW SOUTH WALES, 2327 AUSTRALIA
1	AGENCY FOR DEFENSE DEVELOPMENT JAIMIN LEE YUSEONG PO BOX 35 (1-3-7) TAEJON, 305-600 KOREA
1	COMMISSARIAT A L'ENERGIE ATOMIQUE JEAN-PAUL PLOTARD COURTRY, 77181 FRANCE
2	FRENCH-GERMAN RESEARCH INSTITUTE (ISL) HENRY P. A. MOULARD MICHEL M. S. SAMIRANT 5 RUE DE GENERAL CASSAGNOU SAINT-LOUIS CEDEX, 68301 FRANCE
1	DEFENCE RESEARCH ESTABLISHMENT, VALCARTIER CONRAD BELANGER 2459 PIE XI BOULEVARD NORTH QUEBEC, GOA 1R0 CANADA
1	DEFENCE RESEARCH AGENCY PETER J. HASKINS FORT HALSTEAD SEVENOAKS, KENT TN14 7BP ENGLAND
1	ATOMIC WEAPONS ESTABLISHMENT (FOULNESS) HUGH R. JAMES FOULNESS ISLAND SOUTHEND-ON-SEA, ESSEX, SS3 9XE ENGLAND

REPORT DOCUMENTATION PAGE

Form Approved
OMB No. 0704-0188

1. AGENCY USE ONLY *(Leave blank)*	2. REPORT DATE	3. REPORT TYPE AND DATES COVERED
	May 1998	Final, 1 Oct 95 - 30 Jun 97

4. TITLE AND SUBTITLE
An Assessment of the Performance of the History Variable Reactive Burn Explosive Initiation Model in the CTH Code

5. FUNDING NUMBERS
1L162618AH80

6. AUTHOR(S)
John Starkenberg and Toni M. Dorsey

7. PERFORMING ORGANIZATION NAME(S) AND ADDRESS(ES)
U.S. Army Research Laboratory
ATTN: AMSRL-WM-TB
Aberdeen Proving Ground, MD 21010-5423

8. PERFORMING ORGANIZATION REPORT NUMBER

9. SPONSORING/MONITORING AGENCY NAMES(S) AND ADDRESS(ES)

10.SPONSORING/MONITORING AGENCY REPORT NUMBER

11. SUPPLEMENTARY NOTES

12a. DISTRIBUTION/AVAILABILITY STATEMENT
Approved for public release; distribution is unlimited.

12b. DISTRIBUTION CODE

13. ABSTRACT *(Maximum 200 words)*

We exercised the History Variable Reactive Burn (HVRB) model in the CTH code, simulating a number of common explosive sensitivity experiments, including sustained- and pulsed-shock initiation, projectile-impact initiation, and detonation failure. Predictions of sustained-shock initiation are accurate in accordance with the calibration of the model. Predictions of pulsed-shock initiation are only somewhat more accurate than those achieved previously using Forest Fire. Predictions of projectile-impact initiation are much better. The results for bare explosive show excellent agreement with experiment for both flat- and round-tipped projectiles. With a 2-mm tantalum cover, the agreement is nearly as good. With a 6-mm tantalum cover, the agreement deteriorates for flat-tipped projectiles, while remaining adequate in the case of round-tipped projectiles. The failure radius and thickness predicted with CTH exhibit minimam (near which the solutions are most stable) as functions of zone dimension, but do not appear to converge. These minimum values agree well with experiment. Although no converged solutions were obtained, the most stable failure thickness is approximately equal to the most stable failure radius.

14. SUBJECT TERMS
explosives, detonation, initiation, projectile impact, critical diameter

15. NUMBER OF PAGES
52

16. PRICE CODE

17. SECURITY CLASSIFICATION OF REPORT	18. SECURITY CLASSIFICATION OF THIS PAGE	19. SECURITY CLASSIFICATION OF ABSTRACT	20. LIMITATION OF ABSTRACT
UNCLASSIFIED	UNCLASSIFIED	UNCLASSIFIED	UL

INTENTIONALLY LEFT BLANK.

USER EVALUATION SHEET/CHANGE OF ADDRESS

This Laboratory undertakes a continuing effort to improve the quality of the reports it publishes. Your comments/answers to the items/questions below will aid us in our efforts.

1. ARL Report Number/Author ARL-TR-1667 (Starkenberg) Date of Report May 1998

2. Date Report Received _____

3. Does this report satisfy a need? (Comment on purpose, related project, or other area of interest for which the report will be used.) _____

4. Specifically, how is the report being used? (Information source, design data, procedure, source of ideas, etc.) _____

5. Has the information in this report led to any quantitative savings as far as man-hours or dollars saved, operating costs avoided, or efficiencies achieved, etc? If so, please elaborate. _____

6. General Comments. What do you think should be changed to improve future reports? (Indicate changes to organization, technical content, format, etc.) _____

CURRENT ADDRESS

Organization

Name E-mail Name

Street or P.O. Box No.

City, State, Zip Code

7. If indicating a Change of Address or Address Correction, please provide the Current or Correct address above and the Old or Incorrect address below.

OLD ADDRESS

Organization

Name

Street or P.O. Box No.

City, State, Zip Code

(Remove this sheet, fold as indicated, tape closed, and mail.)

(DO NOT STAPLE)